Detecting Protein-Glycolipid Interactions using Glycomicelles and CaR-ESI-MS

Ling Han, Elena N. Kitova and John S. Klassen*

Alberta Glycomics Centre and Department of Chemistry,

University of Alberta, Edmonton, Alberta, Canada T6G 2G2

*Corresponding Author's address:

Department of Chemistry, University of Alberta

Edmonton, AB CANADA T6G 2G2

Email: john.klassen@ualberta.ca

Telephone: (780) 492-3501

Abstract

This study reports on the use of the catch-and-release electrospray ionization mass spectrometry (CaR-ESI-MS) assay, combined with glycomicelles, as a method for detecting specific interactions between water-soluble proteins and glycolipids (GLs) in aqueous solution. The B subunit homopentamers of cholera toxin (CTB_5) and Shiga toxin type 1 B ($Stx1B_5$) and the gangliosides GM1, GM2, GM3, GD1a, GD1b, GT1b and GD2 served as model systems for this study. The CTB_5 exhibits broad specificity for gangliosides and binds to GM1, GM2, GM3, GD1a, GD1b, GT1b; $Stx1B_5$ does not recognize gangliosides. The CaR-ESI-MS assay was used to analyze solutions of CTB_5 or $Stx1B_5$ and individual gangliosides (GM1, GM2, GM3, GD1a, GD1b, GT1b and GD2) or mixtures thereof. The high affinity interaction of CTB_5 with GM1 was successfully detected. However, the apparent affinity, as determined from the mass spectra, is significantly lower than that of the corresponding pentassacharide or when GM1 is presented in model membranes such as nanodiscs. Interactions between CTB_5 and the low affinity gangliosides GD1a, GD1b and GT1b, as well as GD2, which served as a negative control, were detected; no binding of CTB_5 to GM2 or GM3 was observed. The CaR-ESI-MS results obtained for $Stx1B_5$ reveal that non-specific protein-ganglioside binding can occur during the ESI process, although the extent of binding varies between gangliosides. Consequently, interactions detected for CTB_5 with GD1a, GD1b and GT1b are likely non-specific in origin. Taken together, these results reveal that the CaR-ESI-MS/glycomicelle approach for detecting protein-GL interactions is prone to false positives and false negatives and must be used with caution.

Introduction

Cell-surface glycolipids (GLs) are involved in a number of critical cellular processes including recognition and adhesion, pathogen infection, signal transduction, trafficking, and immune response [1-3]. Glycolipids are amphipathic molecules consisting of a hydrophobic lipid moiety, which inserts into the cell membrane, and a hydrophilic mono-, oligo- or polysaccharide head group that is exposed to the aqueous environment. Glycolipids are readily immobilized on hydrophobic surfaces and, thus, their interactions with water-soluble proteins can be studied using enzyme-linked immunosorbent assay (ELISA), surface plasmon resonance (SPR) spectroscopy, and thin layer chromatography (TLC) [4-6]. In addition, microarrays prepared using naturally-occurring GLs or synthetic GLs (neoGLs), which enable GL-based glycan screening, have been successfully used for the discovery of protein-GL interactions [7-9]. However, a shortcoming of these methods is the non-native environment of the GLs, which could influence the nature of protein-GL interactions. An alternative approach is to incorporate the GLs in a lipid monolayer or bilayer, such that the protein-GL interactions can be studied in a more native-like environment [10]. For such studies, a variety of different model membranes have been used to solubilize the GLs, including supported lipid bilayers, liposomes, micelles, bicelles, nanodiscs, and picodiscs [11-14], and the protein-GL interactions probed using diverse analytical techniques (e.g., fluorescence, nuclear magnetic resonance (NMR) and SPR spectroscopy) [15-18].

Recently, electrospray ionization mass spectrometry (ESI-MS) has emerged as a promising method for the studying of protein-GL interactions in aqueous solution. Interactions between water-soluble lectins and GLs, solubilized using nanodiscs (NDs), have been detected using the catch-and-release (CaR)-ESI-MS assay [19,20]. Nanodiscs are discoidal phospholipid bilayers

surrounded by two copies of an amphipathic membrane scaffold protein [12,13]. It was also shown that NDs can serve as GL arrays and be combined with the CaR-ESI-MS assay to rapidly screen mixtures of GLs (defined or natural libraries) against target proteins [21]. The successful detection of both high and low affinity protein-GL interactions using this approach has been reported [21]. The CaR-ESI-MS assay has also been combined with picodiscs (PDs) [14], which are smaller lipid-transporting macromolecular complexes composed of the human sphingolipid activator protein, saposin A (SapA) and phospholipids, for the detection of protein-GL complexes [22,23]. More recently, Zamfir and coworkers reported on the detection of interactions between proteins and gangliosides (which are glycosphingolipids that contain sialic acid) in aqueous solution using direct ESI-MS analysis [24]. Using this approach, in which the gangliosides presumably form GL micelles (glycomicelles) in solution, the authors identified the interactions between B subunits of cholera toxin (CTB) and GM1, GD1, GT1, GQ1, GP1, as well as the fucosylated GD1, GT1 and GQ1 [24]. However, it is notable that these measurements were carried out at acidic pH (5.8), conditions under which the native homopentameric structure of CTB (i.e., CTB_5) disassembles into individual subunits. Given that the ganglioside binding pocket, as identified from the X-ray crystal structure [25], is comprised of residues from adjacent B subunits, the nature of the interactions involving a single subunit is unclear.

Given the versatility and ease of implementation, the ESI-MS approach, performed directly on aqueous solutions of protein and GL, for detecting protein-GL interactions is very attractive. The goal of the present study was to more thoroughly investigate the reliability of using ESI-MS (and CaR-ESI-MS) and glycomicelles to detect protein–GL interactions. The B subunit homopentamers of cholera toxin (CTB_5) and Shiga toxin type 1 ($Stx1B_5$) and seven gangliosides (GM1, GM2, GM3, GD1a, GD1b, GT1b and GD2) served as model systems for this study. CTB_5

exhibits broad specificity for gangliosides (sialic acid containing GLs); $Stx1B_5$ is known to bind globosides (neutral glycosphingolipids) such as Gb3 and Gb4, but does not recognize gangliosides [26,27]. The CaR-ESI-MS assay, which is outlined in Figure 1, was used to analyze aqueous solutions of CTB_5 or $Stx1B_5$ and individual gangliosides (GM1, GM2, GM3, GD1a, GD1b, GT1b and GD2) or mixtures thereof. With the exception of GM3, which does not form micelles [28,29], the concentrations of gangliosides were above the critical micelle concentration [29,30]. The ganglioside interactions identified for CTB_5 and $Stx1B_5$ by CaR-ESI-MS, together with binding data acquired for CTB_5 and gangliosides solubilized in NDs or PDs, as well as affinity data measured for CTB_5 and the ganglioside oligosaccharides, was used to assess the reliability of using ESI-MS (and CaR-ESI-MS) and glycomicelles for detecting protein-GL interactions in aqueous solutions.

Experimental

Materials and Methods

Proteins

Cholera toxin B subunit homopentamer (CTB_5, MW 58,040 Da) was purchased from Sigma-Aldrich Canada (Oakville, Canada). Shiga toxin type 1 B subunit homopentamer ($Stx1B_5$, MW 38 455 Da) was a gift from Prof. G. Armstrong (University of Calgary). A single chain variable fragment (scFv, MW 26,539 Da) of the monoclonal antibody Se155-4, which served as a reference protein (P_{ref}) [31,32] for direct ESI-MS binding measurements, was produced using recombinant technology as described elsewhere [33]. To prepare stock solutions of CTB_5 and $Stx1B_5$, each protein was dialyzed against 200 mM ammonium acetate (pH 6.8) using 0.5 mL Amicon microconcentrators (EMD Millipore, Billerica, MA) with a 30 kDa MW cutoff. A similar procedure, using microconcentrators with a 10 kDa MW cutoff, was applied to scFv. The

concentration of CTB_5 stock solution was determined using a Pierce BCA assay kit (Thermo Scientific, Ottawa, Canada) following the manufacturer's instruction; the concentrations of the $Stx1B_5$ and scFv solutions were estimated by UV absorption (280 nm). All protein stock solutions were kept at 4 °C until used.

Gangliosides

The gangliosides β-D-Gal-(1,3)-β-D-GalNAc-(1,4)-[α-D-Neu5Ac-(2,3)]-β-D-Gal-(1,4)-β-D-Glc-ceramide (GM1, major isoforms *d*18:1-18:0 and *d*20:1-18:0 have MWs 1545.88 Da, 1573.91 Da), β-D-GalNAc-(1,4)-[α-D-Neu5Ac-(2,3)]-β-D-Gal-(1,4)-β-D-Glc-ceramide (GM2, major isoforms *d*18:1-18:0 and *d*20:1-18:0 have MWs 1383.82 Da, 1411.86 Da) and α-D-Neu5Ac-(2,3)-β-D-Gal-(1,4)-β-D-Glc-ceramide (GM3, major isoforms *d*18:1-18:0 and *d*20:1-18:0 have MWs 1180.74 Da, 1208.78 Da) were purchased from Cedarlane Labs (Burlington, Canada); α-D-Neu5Ac-(2,3)-β-D-Gal-(1,3)-β-D-GalNAc-(1,4)-[α-D-Neu5Ac-(2,3)]-β-D-Gal-(1,4)-β-D-Glc-ceramide (GD1a, major isoforms *d*18:1-18:0 and *d*20:1-18:0 have MWs 1836.97 Da, 1865.00 Da), (β-D-Gal-(1,3)-β-D-GalNAc-(1,4)-[α-D-Neu5Ac-(2,8)-α-D-Neu5Ac-(2,3)]-β-D-Gal-(1,4)-β-D-Glc-ceramide (GD1b, major isoforms *d*18:1-18:0 and *d*20:1-18:0 have MWs 1836.97 Da, 1865.00 Da), α-Neu5Ac-(2-3)-β-D-Gal-(1-3)-β-D-GalNAc-(1-4)-[α-Neu5Ac-(2-8)-α-Neu5Ac-(2-3)]-β-D-Gal-(1-4)-β-D-Glc-ceramide (GT1b, major isoforms *d*18:1-18:0 and *d*20:1-18:0 have MWs 2128.07 Da, 2156.10 Da) were purchased from Sigma-Aldrich Canada (Oakville, Canada), and β-D-GalNAc-(1,4)-[α-D-Neu5Ac-(2,8)-α-D-Neu5Ac-(2,3)]-β-D-Gal-(1,4)-β-D-Glc-ceramide (GD2, major isoforms *d*18:1-18:0 and *d*20:1-18:0 have MWs 1674.92 Da, 1702.95 Da) were purchased from MyBioSource Inc. (San Diego, CA). The structures of the gangliosides are given in Figure S1 (Supporting Information).

Stock solutions (2 mM) of each ganglioside in HPLC grade methanol/chloroform (1:1, v/v, Thermo Fisher, Ottawa, Canada) were prepared and stored at −20 °C until needed.

Oligosaccharides

The ganglioside oligosaccharides β-D-Gal-(1,3)-β-D-GalNAc-(1,4)-[α-D-Neu5Ac-(2,3)]-β-D-Gal-(1,4)-D-Glc ($GM1_{os}$, MW 998.34 Da); β-D-GalNAc-(1,4)-[α-D-Neu5Ac-(2,3)]-β-D-Gal-(1,4)-D-Glc ($GM2_{os}$, MW 836.29 Da); α-D-Neu5Ac-(2,3)-β-D-Gal-(1,4)-D-Glc ($GM3_{os}$, MW 633.21 Da); α-D-Neu5Ac-(2,3)-β-D-Gal-(1,3)-β-D-GalNAc-(1,4)-[α-D-Neu5Ac-(2,3)]-β-D-Gal-(1,4)-D-Glc ($GD1a_{os}$, MW 1289.44 Da); β-D-Gal-(1,3)-β-D-GalNAc-(1,4)-[α-D-Neu5Ac-(2,8)-α-D-Neu5Ac-(2,3)]-β-D-Gal-(1,4)-D-Glc ($GD1b_{os}$, MW 1289.44 Da); β-D-GalNAc-(1,4)-[α-D-Neu5Ac-(2,8)-α-D-Neu5Ac-(2,3)]-β-D-Gal-(1,4)-D-Glc ($GD2_{os}$, MW 1127.39 Da); α-Neu5Ac-(2-3)-β-D-Gal-(1-3)-β-D-GalNAc-(1-4)-[α-Neu5Ac-(2-8)-α-Neu5Ac-(2-3)]-β-D-Gal-(1-4)-D-Glc ($GT1b_{os}$, MW 1580.53 Da) were purchased from Elicityl SA (Crolles, France). The structures of the oligosaccharides are shown in Figure S2 (Supporting Information). Stock solutions (1 mM in Milli-Q water (Millipore, MA)) of each of the oligosaccharides were stored at -20 °C until needed.

Preparation of glycolipid micelles

To prepare micellar solutions, the ganglioside (or ganglioside mixture) was diluted in 1:1 methanol/chloroform and dried under gentle stream of nitrogen to form a lipid film. The dried lipid film was stored at room temperature overnight. Subsequently, the lipid film was re-suspended in 200 mM aqueous ammonium acetate solution (pH 6.8, 25 °C) by vortexing for 5 min, followed by 30 min of sonication [18]. The resulting solution was stored at room temperature until used.

Mass spectrometry

ESI-MS measurements were carried out using a Waters Synapt G2S quadrupole-ion mobility separation-time of flight (Q-IMS-TOF) mass spectrometer (Manchester, UK) equipped with a nanoflow ESI (nanoESI) source. Sample solutions were prepared in 200 mM aqueous ammonium acetate buffer (pH 6.8, 25°C) and each solution was loaded into a nanoESI tip, which was produced by pulling the borosilicate capillaries (1.0 mm o.d., 0.68 mm i.d.) to ~5 µm using a P-1000 micropipette puller (Sutter Instruments, Novato, CA). To perform nanoESI, a voltage of -0.8 kV (negative ion mode) or 1.0 kV (positive ion mode) was applied to a platinum wire inserted into the nanoESI tip. For the ESI-MS measurements, the source temperature was 60 °C, the cone voltage was 50 V (negative ion mode) or 35 V (positive ion mode) and the Trap and Transfer voltages were 5 and 2 V, respectively. For the CaR-ESI-MS measurements, the quadrupole mass filter was set to pass a window of ions corresponding to the complexes of interest (using quadrupole parameters of LM = 8, HM = 15, window width ~50 m/z units; LM = 4, HM = 15, window width ~100 m/z units; or LM = 2, HM = 15, window width ~200 m/z units). Collision-induced dissociation (CID) was performed in the Trap using argon (2.15×10^{-2} mbar) and 100 V collision energy. All data were processed using MassLynx software (version 4.1).

The abundances of free and GL-bound protein ions were calculated from the ESI mass spectra using peak heights (intensities), with no background subtraction performed. Details of the procedure used to calculate the normalized distributions of free and GL-bound proteins have been reported previously [20]. The quantitative binding measurements performed on $Stx1B_5$ and the ganglioside oligosaccharides were carried out using the direct ESI-MS assay. A detailed description of the method can be found elsewhere [31,32]. For these measurements, a P_{ref} was added to the solutions in order to quantitatively correct the mass spectra for the occurrence of

nonspecific protein-carbohydrate binding during the ESI process. A description of the correction method and its implementation is reported elsewhere [31,32].

Results and Discussion

In the present study, the interactions of CTB_5 and $Stx1B_5$ with seven different gangliosides (GM1, GM2, GM3, GD1a, GD1b, GD2 and GT1b), either alone or present as an equimolar mixture in aqueous solution, were studied using CaR-ESI-MS. With the exception of GM3 (which forms large vesicles at concentrations >3 nM) [28,29], each of the gangliosides is expected to form micelles in aqueous solution at the concentrations used. The critical micelle concentrations (CMC) of GM1, GM2, GD1a, GD1b and GT1b are reported as: 20 nM, 11 nM, 2 μM, 1 μM and 10 μM, respectively [29,30]. To our knowledge the CMC for GD2 has not been reported. However, given the structural similarity between GD2 and GD1a/b, the CMC of GD2 is likely 1 – 2 μM.

Shown in Figure S3 (Supporting Information) are representative ESI mass spectra acquired in negative ion mode for aqueous ammonium acetate solutions (200 mM, pH 6.8, 25 °C) of 400 μM of GM1, GM2, GD1a, GD1b, GT1b or GD2. In each case, a broad feature, centred at m/z 7,000 – 10,000, is evident. This feature, which is qualitatively similar to the results obtained by ESI-MS analysis on the detergent micelles, is attributed to the ganglioside micelle ions [34-36]. The ESI mass spectrum acquired for GM3 also exhibit a broad feature, centered at m/z 13,000 – 16,000, although with lower abundance (Figure S3m, Supporting Information). This finding is consistent with the fact that GM3 tends to form large vesicles [28,29]. The confirm the presence of each ganglioside, CID was performed on ions with a range of m/z values (window width ~200 m/z units) centered at an m/z corresponding to the most abundant micellar ions. In each case,

signal corresponding to the deprotonated ions of each of the gangliosides was detected (Figures S3b, d, f, h, j, l and n, Supporting Information).

The high affinity interactions between CTB_5 and GM1 served as a starting point for testing the reliability of the CaR-ESI-MS assay, implemented with glycomicelles, for detecting protein interactions with GLs *in vitro*. Measurements were performed on aqueous ammonium acetate solutions (200 mM, pH 6.8, 25 °C) of CTB_5 (3 μM) and GM1, at concentrations ranging from 20 to 360 μM. Shown in Figure 2 are representative ESI mass spectra measured for three GM1 concentrations, 20 μM, 80 μM and 360 μM. At lowest concentration investigated (20 μM), only signal corresponding to free CTB_5 ions, i.e., CTB_5^{n-} at n = 13 – 16, was evident in the mass spectrum. Moreover, there was no obvious signal that could be attributed to GM1 micelle ions. CID performed using a ~50 m/z window centered at m/z 4,587, which corresponds to the -13 charge state of the putative (CTB_5 + GM1) complex, resulted in the appearance of B subunit monomer ions (at charge states -5 and -6) and GM1 ions, albeit at very low abundance (Figure 2b). Analogous CID measurements performed using identical experimental conditions, but in the absence of CTB_5, failed to produce any detectable signal corresponding to GM1 (Figure S4, Supporting Information). Taken together, these results indicate that CTB_5–GM1 interactions exist in solution, but are presumably at very low concentration. At higher concentrations of GM1 (Figures 2c and 2e), signal consistent with complexes of CTB_5 bound to one or more GM1 molecules was detected, i.e., $(CTB_5 + qGM1)^{n-}$ with q = 2 – 5 and n = 13 – 16 (Table S1, Supporting Information), and the number of bound GM1 increased with GM1 concentration. The presence of bound GM1 was also confirmed by CID, performed using conditions identical to those described above (Figures 2d and 2f). It can also be seen that signal corresponding to GM1 micelle ions becomes more abundant with increasing ganglioside concentration (Figure 2e).

The normalized distributions of (CTB_5 + *q*GM1) species determined from the mass spectra and the corresponding distributions expected for the GM1 pentasaccharide ($GM1_{os}$), which were calculated based on the reported apparent affinities for the stepwise binding of $GM1_{os}$ to CTB_5, at the same concentration as GM1 are shown in Figures 2a, 2c and 2e [37,38]. Notably, at 20 μM $GM1_{os}$, CTB_5 is expected to be almost fully bound, whereas CTB_5 appears to exist almost exclusively in the unbound form at 20 μM GM1 micelle (Figure 2a). At $GM1_{os}$ concentrations >30 μM, CTB_5 is essentially fully bound; in contrast, a significant fraction of the binding sites remain unoccupied even at GM1 concentrations as high as >80 μM (Figure 2c). The effect of concentration is, perhaps, more clearly seen in Figure 2g, where the fraction (*f*) of occupied CTB_5 binding sites is plotted versus GM1 concentration. Also shown is the fraction of occupied binding sites expected for $GM1_{os}$ at concentrations between 0 and 370 μM and the fraction of bound CTB_5 measured experimentally using NDs to solubilize GM1 [20]. It can be seen that *f* appears to reach a limiting value of ~0.85 at GM1 concentrations >200 μM, which contrasts with an *f* of 0.99 at 30 μM $GM1_{os}$. It is also important to note that the significantly higher concentrations of GM1 are required to achieve near saturation (of the binding sites) compared to the case when GM1-containing NDs are used, wherein an *f* of ~0.9 is reached at GM1 concentrations of ~30 μM [20].

To confirm that nonspecific binding between CTB_5 and GM1 during the ESI process (due to concentration effects in the droplets) does not contribute appreciably to the measured distributions of (CTB_5 + *q*GM1) species, analogous CaR-ESI-MS measurements were performed using $Stx1B_5$, which, to the best of our knowledge, does not bind to gangliosides. To further support the use of $Stx1B_5$ as a negative control, binding measurements were carried on the GM1 pentasaccharide ($GM1_{os}$), as well as the oligosaccharides of the six other gangliosides using the

direct ESI-MS assay in positive ion mode (Figure S5, Supporting Information). Notably, no interactions between $Stx1B_5$ and $GM1_{os}$ or to the other six oligosaccharides were detected. Application of CaR-ESI-MS to an aqueous ammonium acetate solution (200 mM, pH 6.8, 25 °C) of $Stx1B_5$ (3 μM) with GM1 (360 μM) produced no evidence of the presence of ($Stx1B_5$ + *q*GM1) complexes, either directly (Figure S6a, Supporting Information) or by release of bound ganglioside by CID (Figure S6b, Supporting Information). These results suggest that nonspecific binding of CTB_5 and GM1 during the ESI process does not contribute in a meaningful way to the mass spectrum. Based on these findings it is concluded that the (CTB_5 + *q*GM1) complexes detected by ESI-MS are the result of specific interactions between CTB_5 and GM1 micelles in solution. Moreover, the measured distributions of (CTB_5 + *q*GM1) species suggest that the affinity of GM1, when present as a glycomicelle, for CTB_5 is significantly lower than when GM1 is presented in a ND [20]. While the origin of the reduced affinity can't be elucidated based on the present experimental data, it is reasonable to conclude that it arises from differences in the oligosaccharide environment when presented in micelles and NDs.

The results obtained for CTB_5 and GM1 demonstrate that high affinity protein-GL interactions can be detected directly by ESI-MS performed on solutions containing lectin and GL. However, significantly higher GL concentrations are required in order to achieve the same extent of binding as compared to the corresponding GL oligosaccharide or when using NDs (or PDs) to solubilize the GLs [37,20,22]. The next step was to establish whether low affinity protein-GL interactions could be detected. To answer this question, the CaR-ESI-MS assay was applied to aqueous ammonium acetate solutions (200 mM, pH 6.8, 25 °C) of CTB_5 (3 μM) and GM2, GM3, GD1a, GD1b or GT1b. The affinities measured for the oligosaccharides $GM2_{os}$, $GM3_{os}$, $GD1a_{os}$, GD1b and GT1b are approximately three orders of magnitude lower than for the GM1

pentasaccharide [23]. Shown in Figures S7 and S8 (Supporting Information) are representative mass spectra measured for solutions containing CTB_5 with GM2 and GM3, respectively. Surprisingly, no interaction between CTB_5 and either of these gangliosides was detected, even at concentrations as high as 360 μM ganglioside. In contrast, binding of CTB_5 to GD1a, GD1b and to GT1b was readily detected by CaR-ESI-MS and the measured distributions of free and bound CTB_5 are similar to those predicted, based on the reported affinities, for the corresponding oligosaccharides (Figures S9 – S11, Supporting Information) [23].

Measurements were also performed on solutions containing CTB_5 with GD2, which served as a negative control. Direct ESI-MS binding measurements carried out on the GD2 pentasaccharide ($GD2_{os}$) and CTB_5 revealed no evidence of binding [23]. The results of an SPR spectroscopy binding study also suggest that CTB_5 does not bind to GD2 liposomes [39]. Moreover, application of the CaR-ESI-MS assay to solutions of CTB_5 and GD2, incorporated into NDs or PDs, failed to identify any binding [21,23]. Shown in Figure S12 (Supporting Information) are representative CaR-ESI-MS data acquired for aqueous ammonium acetate solutions (200 mM, pH 6.8, 25 °C) of CTB_5 (3 μM) and GD2 at 80 μM and 200 μM. Unexpectedly, signal corresponding to the (CTB_5 + GD2) complex is clearly evident in both ESI mass spectra (Figures S12a and S12c, Supporting Information). Collision-induced dissociation performed on the ions of the (CTB_5 + GD2) complex conclusively established the presence of bound GD2 (Figures S12b and S12d, Supporting Information).

The results of the CaR-ESI-MS measurements performed on solutions of CTB_5 and seven gangliosides are intriguing and, seemingly, contradictory. The absence of detectable binding to the low affinity ligands, GM2 and GM3 could be explained, in principle, by a reduced affinity resulting from the micellar presentation of these gangliosides. This explanation finds support in

the results obtained for GM1, *vide supra*. However, the finding that GD1a, GD1b and GT1b exhibit affinities that are apparently similar to those of the corresponding oligosaccharides is at odds with this general explanation. Moreover, the detection of CTB_5 binding to GD2, which is a negative control, adds further confusion to the situation.

In an effort to make sense of these observations, CaR-ESI-MS measurements were performed on aqueous ammonium acetate solutions (200 mM, pH 6.8, 25 °C) of $Stx1B_5$ (3 μM) and each of the six gangliosides – GM2, GM3, GD1a, GD1b, GT1b and GD2 (at 320 μM). As expected, no binding of $Stx1B_5$ to GM2 (Figure S13, Supporting Information) or GM3 (Figure S14, Supporting Information) was observed. However, binding was detected for GD1a, GD1b, GT1b and GD2 (Figures S15 – S18, Supporting Information). To facilitate comparison of these results with those obtained for CTB_5, the normalized distributions of ligand (ganglioside or ganglioside oligosaccharide)-bound CTB_5 and $Stx1B_5$ measured for each ganglioside or ganglioside oligosaccharide are given in Figure S19 (Supporting Information).

As discussed above, $Stx1B_5$ exhibits no measurable affinity for the oligosaccharides of these gangliosides. Consequently, the identified interactions are likely formed during the ESI process as a result of non-specific interactions. The absence of non-specific binding observed for GM2 and GM3 (as well as GM1, *vide supra*) is likely due to the very low CMC for these gangliosides [29], which presumably translates to a very low concentration of free ganglioside in solution. It is also possible that in-source (i.e., gas-phase) dissociation may be responsible for the absence of observed binding for these protein-ganglioside complexes. The CaR-ESI-MS results obtained for $Stx1B_5$ and GD2 also provide a possible explanation for the observation of CTB_5 binding to GD2. The occurrence of non-specific binding could also explain the unexpected distributions of bound GD1a, GD1b and GT1b observed for CTB_5.

The aforementioned results suggest that the environment of ganglioside oligosaccharides in glycomicelles influences lectin binding in solution. To further probe this phenomenon, the CaR-ESI-MS assay was applied to solutions containing CTB_5 and all seven of the gangliosides. Shown in Figure 3 are ESI mass spectra acquired for aqueous ammonium acetate solutions (200 mM, pH 6.8, 25 °C) of CTB_5 (3 μM) with GM1, GM2, GM3, GD1a, GD1b, GT1b and GD2, each at 80 μM (Figure 3a) or 150 μM (Figure 3c) concentrations. The broad feature centered at ~9,000 m/z is attributed to ganglioside micelle ions (Figure S20a, Supporting Information); CID of these ions produced signal corresponding to the anions of GM1, GM2, GM3, GT1b and GD2, as well as GD1 (Figure S20b, Supporting Information). Because GD1a and GD1b are structural isomers, the presence of both gangliosides could not be established simply from the CID mass spectrum. Also identified in the mass spectrum are ions corresponding to $(CTB_5 + q\text{GM1})^{n-}$ with $q = 3 – 5$ and $n = 14 – 16$ (Figures 3a and 3c). Due to the inadequate mass resolution, it is not possible to establish directly whether other gangliosides were also bound to CTB_5. However, CID performed using a ~100 m/z window centered at m/z 4,400, which corresponds approximately to the -15 charge state of CTB_5 bound to five gangliosides, resulted in the appearance of abundant GM1 anions, as well as the anions of GM2, GM3, GD2, GT1b and GD1 (GD1a/GD1b), but at lower abundance (Figures 3b and 3d). Notably, analogous CID experiments performed on a solution containing the same mixture of gangliosides but in the absence of CTB_5, failed to produce signal corresponding to the ganglioside anions (Figure S20c, Supporting Information). Taken together, these results suggest that the ganglioside ions identified by CID were originally bound to CTB_5.

The aforementioned observation that CTB_5 binds to GM2 and GM3 is surprising given that these gangliosides could not be detected from similar measurements performed on solutions

containing the individual gangliosides, *vide supra*. One possible explanation for this finding is that CTB_5-ganglioside binding (specific or non-specific) is enhanced by the presence of the high affinity GM1 ligand. In other words, it is possible that GM1 anchors CTB_5 to the micelle allowing the protein to interact, either specifically (in solution) or non-specifically (during the ESI process), with other gangliosides that are present in the micelle. To test this hypothesis, the CaR-ESI-MS assay was also carried out for aqueous ammonium acetate solutions (200 mM, pH 6.8, 25 °C) of CTB_5 (3 μM) with GM2, GM3, GD1b and GD2, each at 160 μM (Figure 4a) and 290 μM (Figure 4c). It can be seen that, in the absence of GM1, very little ganglioside-bound CTB_5 was detected (Figures 4a and 4c). CID performed using a ~100 m/z window centered at m/z 4,605, which corresponds approximately to the -13 charge state of CTB_5 bound to a single ganglioside (Figures 4b and 4d), produced predominantly signal corresponding to GD1b and GD2, with GM2 and GM3 anions present at very low abundance. These results, taken together with those shown in Figure 3, suggest that the high affinity interaction between CTB_5 and GM1 promotes binding of CTB_5 to the other gangliosides. It is also possible that the presence of GM1 leads to a more favourable presentation of the other glycolipids in the micelles.

Conclusions

The present study represents the first comprehensive investigation into the detection of protein-GL interactions in aqueous solution using glycomicelles and the CaR-ESI-MS assay. The high affinity interaction between CTB_5 and GM1 was successfully detected. However, the apparent affinity, as determined from the mass spectrum, is significantly lower than that of the corresponding ganglioside pentasaccharide or when GM1 is present in model membranes, such as nanodiscs or picodiscs. Interactions between CTB_5 and the low affinity ganglioside ligands GM2, GM3, GD1a, GD1b and GT1b could not be positively identified by CaR-ESI-MS. No

interaction with GM2 or GM3 was detected. Although interactions were identified for GD1a, GD1b and GT1b, binding was also detected for GD2, which is not recognized by CTB_5. It is proposed that non-specific binding during the ESI process is responsible for the interactions with GD1a, GD1b and GT1b, as well as GD2. This conclusion is supported by the CaR-ESI-MS results obtained for $Stx1B_5$, which revealed the occurrence of non-specific protein-ganglioside binding during ESI. Overall, the results of this study suggest that the CaR-ESI-MS/glycomicelle approach for detecting protein-GL interactions *in vitro* is prone to false positives and false negatives and, therefore, must be used with caution.

Acknowledgement

The authors would like to acknowledge the Natural Sciences and Engineering Research Council of Canada and the Alberta Glycomics Centre for generous funding and Prof. G. Armstrong (University of Calgary) for generously providing protein used in this study.

References

1. Hakomori, S.: Structure, organization, and function of glycosphingolipids in membrane. Curr. Opin. Hematol. **10**, 16-24 (2003)
2. Varki, A.; Cummings, R.D.; Esko, J.D.; Freeze, H.H.; Stanley, P.; Bertozzi, C.R.; Hart, G.W.; Etzler, M.E. Essentials of glycobiology 2nd Ed. Cold Spring Harbor Laboratory Press, Cold Spring Harbor, New York, NY (2009)
3. Schulze, H., Sandhoff, K.: Sphingolipids and lysosomal pathologies. Biochim. Biophys. Acta. **1841**, 799-810 (2014)
4. Evans, S.V., Roger MacKenzie, C.: Characterization of protein–glycolipid recognition at the membrane bilayer. J. Mol. Recognit. **12**, 155-168 (1999)
5. Lopez, P.H., Schnaar, R.L.: Determination of glycolipid-protein interaction specificity. Methods Enzymol. **417**, 205-220 (2006)
6. Kleinschmidt, J. H. Ed. Lipid-protein interactions: Methods and protocols, **974**, Springer: New York, NY (2013)
7. Catimel, B., Scott, A.M., Lee, F.T., Hanai, N., Ritter, G., Welt, S., Old, L.J., Burgess, A.W., Nice, E.C.: Direct immobilization of gangliosides onto gold-carboxymethyldextran sensor surfaces by hydrophobic interaction: applications to antibody characterization. Glycobiology **8**, 927-938 (1998)
8. Feizi, T., Chai, W.: Oligosaccharide microarrays to decipher the glyco code. Nat. Rev. Mol. Cell. Biol. **5**, 582-588 (2004)
9. Song, X., Heimburg-Molinaro, J., Cummings, R.D., Smith, D.F.: Chemistry of natural glycan microarrays. Curr. Opin. Chem. Biol. **18**, 70-77 (2014)
10. Czogalla, A., Grzybek, M., Jones, W., Coskun, U.: Validity and applicability of

membrane model systems for studying interactions of peripheral membrane proteins with lipids. Biochim. Biophys. Acta. **1841**, 1049-1059 (2014)

11. Jayaraman, N., Maiti, K., Naresh, K.: Multivalent glycoliposomes and micelles to study carbohydrate-protein and carbohydrate-carbohydrate interactions. Chem. Soc. Rev. **42**, 4640-4656 (2013)
12. Denisov, I.G., Grinkova, Y.V., Lazarides, A.A., Sligar, S.G.: Directed self-assembly of monodisperse phospholipid bilayer Nanodiscs with controlled size. J. Am. Chem. Soc. **126**, 3477-3487 (2004)
13. Nath, A., Atkins, W.M., Sligar, S.G.: Applications of phospholipid bilayer nanodiscs in the study of membranes and membrane proteins. Biochemistry **46**, 2059-2069 (2007)
14. Popovic, K., Holyoake, J., Pomes, R., Prive, G.G.: Structure of saposin A lipoprotein discs. Proc. Natl. Acad. Sci. U. S. A. **109**, 2908-2912 (2012)
15. Cho, H., Wu, M., Bilgin, B., Walton, S.P., Chan, C.: Latest developments in experimental and computational approaches to characterize protein-lipid interactions. Proteomics **12**, 3273-3285 (2012)
16. Shi, J., Yang, T., Kataoka, S., Zhang, Y., Diaz, A.J., Cremer, P.S.: GM1 clustering inhibits cholera toxin binding in supported phospholipid membranes. J. Am. Chem. Soc. **129**, 5954-5961 (2007)
17. Borch, J., Torta, F., Sligar, S.G., Roepstorff, P.: Nanodiscs for immobilization of lipid bilayers and membrane receptors: kinetic analysis of cholera toxin binding to a glycolipid receptor. Anal. Chem. **80**, 6245-6252 (2008)
18. Yagi-Utsumi, M., Kameda, T., Yamaguchi, Y., Kato, K.: NMR characterization of the interactions between lyso-GM1 aqueous micelles and amyloid β. FEBS Lett. **584**,

831-836 (2010)

19. Zhang, Y., Liu, L., Daneshfar, R., Kitova, E.N., Li, C., Jia, F., Cairo, C.W., Klassen, J.S.: Protein–glycosphingolipid interactions revealed using catch-and-release mass spectrometry. Anal. Chem. **84**, 7618-7621 (2012)

20. Han, L., Kitova, E.N., Li, J., Nikjah, S., Lin, H., Pluvinage, B., Boraston, A.B., Klassen, J.S.: Protein-glycolipid interactions studied in vitro using ESI-MS and nanodiscs: Insights into the mechanisms and energetics of binding. Anal. Chem. **87**, 4888-4896 (2015)

21. Leney, A.C., Fan, X., Kitova, E.N., Klassen, J.S.: Nanodiscs and electrospray ionization mass spectrometry: a tool for screening glycolipids against proteins. Anal. Chem. **86**, 5271-5277 (2014)

22. Leney, A.C., Rezaei Darestani, R., Li, J., Nikjah, S., Kitova, E.N., Zou, C., Cairo, C.W., Xiong, Z.J., Privé, G.G., Klassen, J.S.: Picodiscs for facile protein-glycolipid interaction analysis. Anal. Chem. **87**, 4402-4408 (2015)

23. Li, J., Fan, X., Kitova, E.N., Zou, C., Cairo, C.W., Eugenio, L., Ng, K.K.S., Xiong, Z.J., Privé, G.G., Klassen, J.S.: Screening glycolipids against proteins in vitro using picodiscs and catch-and-release electrospray ionization mass spectrometry. Anal. Chem. **88**, 4742-4750 (2016)

24. Capitan, F., Robu, A.C., Popescu, L., Flangea, C., Vukelić, Ž., Zamfir, A.D.: B subunit monomers of cholera toxin bind G1 ganglioside class as revealed by chip-nanoelectrospray multistage mass spectrometry. J. Carbohydr. Chem. **34**, 388-408 (2015)

25. Merritt, E.A., Kuhn, P., Sarfaty, S., Erbe, J.L., Holmes, R.K., Hol, W.G.J.: The 1.25 Å resolution refinement of the cholera toxin B-pentamer: evidence of peptide backbone

strain at the receptor-binding site1. J. Mol. Biol. **282**, 1043-1059 (1998)

26. Lingwood, C.A., Law, H., Richardson, S., Petric, M., Brunton, J.L., De Grandis, S., Karmali, M.: Glycolipid binding of purified and recombinant Escherichia coli produced verotoxin in vitro. J. Biol. Chem. **262**, 8834-8839 (1987)

27. Gallegos, K.M., Conrady, D.G., Karve, S.S., Gunasekera, T.S., Herr, A.B., Weiss, A.A.: Shiga toxin binding to glycolipids and glycans. PLoS One **7**, e30368 (2012)

28. Sonnino, S., Cantu, L., Acquotti, D., Corti, M., Tettamanti, G.: Aggregation properties of GM3 ganglioside (II3Neu5AcLacCer) in aqueous solutions. Chem. Phys. Lipids. **52**, 231-241 (1990)

29. Sonnino, S., Cantu, L., Corti, M., Acquotti, D., Venerando, B.: Aggregative properties of gangliosides in solution. Chem. Phys. Lipids. **71**, 21-45 (1994)

30. Ulrich-Bott, B., Wiegandt, H.: Micellar properties of glycosphingolipids in aqueous media. J. Lipid Res. **25**, 1233-1245 (1984)

31. Sun, J., Kitova, E.N., Wang, W., Klassen, J.S.: Method for distinguishing specific from nonspecific protein-ligand complexes in nanoelectrospray ionization mass spectrometry. Anal. Chem. **78**, 3010-3018 (2006)

32. Kitova, E., El-Hawiet, A., Schnier, P., Klassen, J.: Reliable determinations of protein–ligand interactions by direct ESI-MS measurements. Are we there yet? J. Am. Soc. Mass. Spectrom. **23**, 431-441 (2012)

33. Zdanov, A., Li, Y., Bundle, D.R., Deng, S.J., Mackenzie, C.R., Narang, S.A., Young, N.M., Cygler, M.: Structure of a single-chain antibody variable domain (Fv) fragment complexed with a carbohydrate antigen at 1.7-Angstrom resolution. Proc. Natl. Acad. Sci. U. S. A. **91**, 6423-6427 (1994)

34. Sharon, M., Ilag, L.L., Robinson, C.V.: Evidence for micellar structure in the gas phase. J. Am. Chem. Soc. **129**, 8740-8746 (2007)

35. Barrera, N.P., Di Bartolo, N., Booth, P.J., Robinson, C.V.: Micelles protect membrane complexes from solution to vacuum. Science **321**, 243-246 (2008)

36. Ilag, L.L., Ubarretxena-Belandia, I., Tate, C.G., Robinson, C.V.: Drug binding revealed by tandem mass spectrometry of a protein-micelle complex. J. Am. Chem. Soc. **126**, 14362-14363 (2004)

37. Lin, H., Kitova, E.N., Klassen, J.S.: Measuring positive cooperativity using the direct ESI-MS assay. Cholera toxin B subunit homopentamer binding to GM1 pentasaccharide. J. Am. Soc. Mass. Spectrom. **25**, 104-110 (2013)

38. Turnbull, W.B., Precious, B.L., Homans, S.W.: Dissecting the cholera toxin-ganglioside GM1 interaction by isothermal titration calorimetry. J. Am. Chem. Soc. **126**, 1047-1054 (2004)

39. MacKenzie, C.R., Hirama, T., Lee, K.K., Altman, E., Young, N.M.: Quantitative analysis of bacterial toxin affinity and specificity for glycolipid receptors by surface plasmon resonance. J. Biol. Chem. **272**, 5533-5538 (1997)

Figure Captions

Figure 1. Schematic representation of the catch-and-release (CaR)-ESI-MS assay for detecting protein-glycolipid interactions using glycomicelles. (a) The soluble carbohydrate-binding protein (P, shown as a homopentameric species) is incubated in aqueous solution with glycomicelles consisting of one or more glycolipid species (L) and analyzed by ESI-MS in negative ion mode. (b) Identification of glycolipid ligands is achieved by subjecting the gaseous protein-glycolipid (PL_i) complexes ions to CID and measuring the MWs of released ligand ions.

Figure 2. ESI mass spectra acquired in negative ion mode for aqueous ammonium acetate solutions (200 mM, 25 °C and pH 6.8) of CTB_5 (3 μM) with GM1 at concentrations of (a) 20 μM, (c) 80 μM, and (e) 360 μM. Insets show the normalized distributions of free and GM1-bound CTB_5; the errors correspond to one standard deviation. Also shown are the distributions of bound $GM1_{os}$ expected based on the association constants reported in reference 37; the errors were calculated from propagation of uncertainties in the reported association constants. (b), (d) and (f) CID mass spectra measured for ions produced by ESI for the solutions described in (a), (c) and (e), respectively. For (b), ions within a window of m/z values (~50 m/z units wide) centred at m/z 4,587 (which corresponds to the -13 charge state of CTB_5 bound to one ganglioside) were isolated; for (d) and (f) ions centred at m/z 4,395 (which corresponds to the -15 charge state of CTB_5 bound to five gangliosides) were isolated; CID was performed in the Trap using a collision energy of 100 V. (g) Plot of fraction of occupied CTB_5 binding sites versus GM1 concentration, as measured by ESI-MS. The 10% GM1 ND binding

data were adapted from reference 20. The dashed line represents the theoretical plot calculated using affinities for the stepwise binding of $GM1_{os}$ to CTB_5 reported in reference 37.

Figure 3. (a) and (c) ESI mass spectra acquired for aqueous ammonium acetate solutions (200 mM, 25 °C and pH 6.8) of CTB_5 (3 μM) and a mixture of GM1, GM2, GM3, GD1a, GD1b, GT1b and GD2, each a concentration of (a) 80 μM and (c) 150 μM. GX represents any of the seven gangliosides. (b) and (d) CID mass spectra measured for ions produced by ESI for the solutions described in (a) and (c), respectively. Ions within a window of m/z values (~100 m/z units wide) centred at 4,400 (which corresponds to the -15 charge state of CTB_5 bound to five gangliosides) were isolated and subjected to CID in the Trap using a collision energy of 100 V.

Figure 4. (a) and (c) ESI mass spectra acquired for aqueous ammonium acetate solutions (200 mM, 25 °C and pH 6.8) of CTB_5 (3 μM) and a mixture of GM2, GM3, GD1a, GD1b, GT1b and GD2, each a concentration of (a) 160 μM and (c) 290 μM. GX represents any of the four gangliosides. (b) and (d) CID mass spectra measured for ions produced by ESI for the solutions described in (a) and (c), respectively. Ions within a window of m/z values (~100 m/z units wide) centred at 4,605 (which corresponds to the -13 charge state of CTB_5 bound to a single ganglioside) were isolated and subjected to CID in the Trap using a collision energy of 100 V.

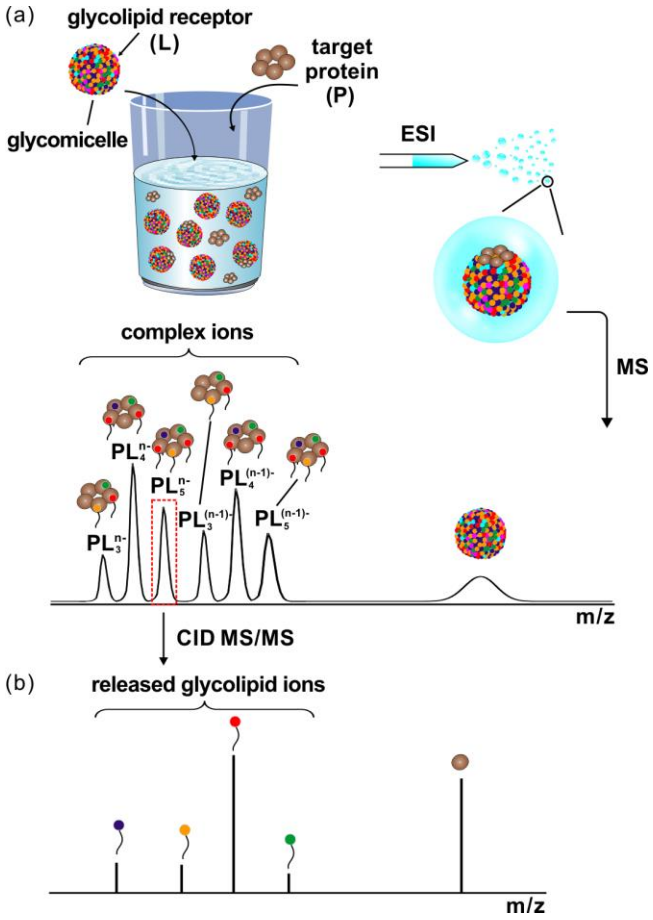
(a)
glycolipid receptor
(L)
target
protein
(P)
glycomicelle
ESI
MS
complex ions
PL_4^{n-}
PL_5^{n-}
PL_3^{n-}
$PL_3^{(n-1)-}$
$PL_4^{(n-1)-}$
$PL_5^{(n-1)-}$
m/z
CID MS/MS
(b)
released glycolipid ions
m/z

Figure 1

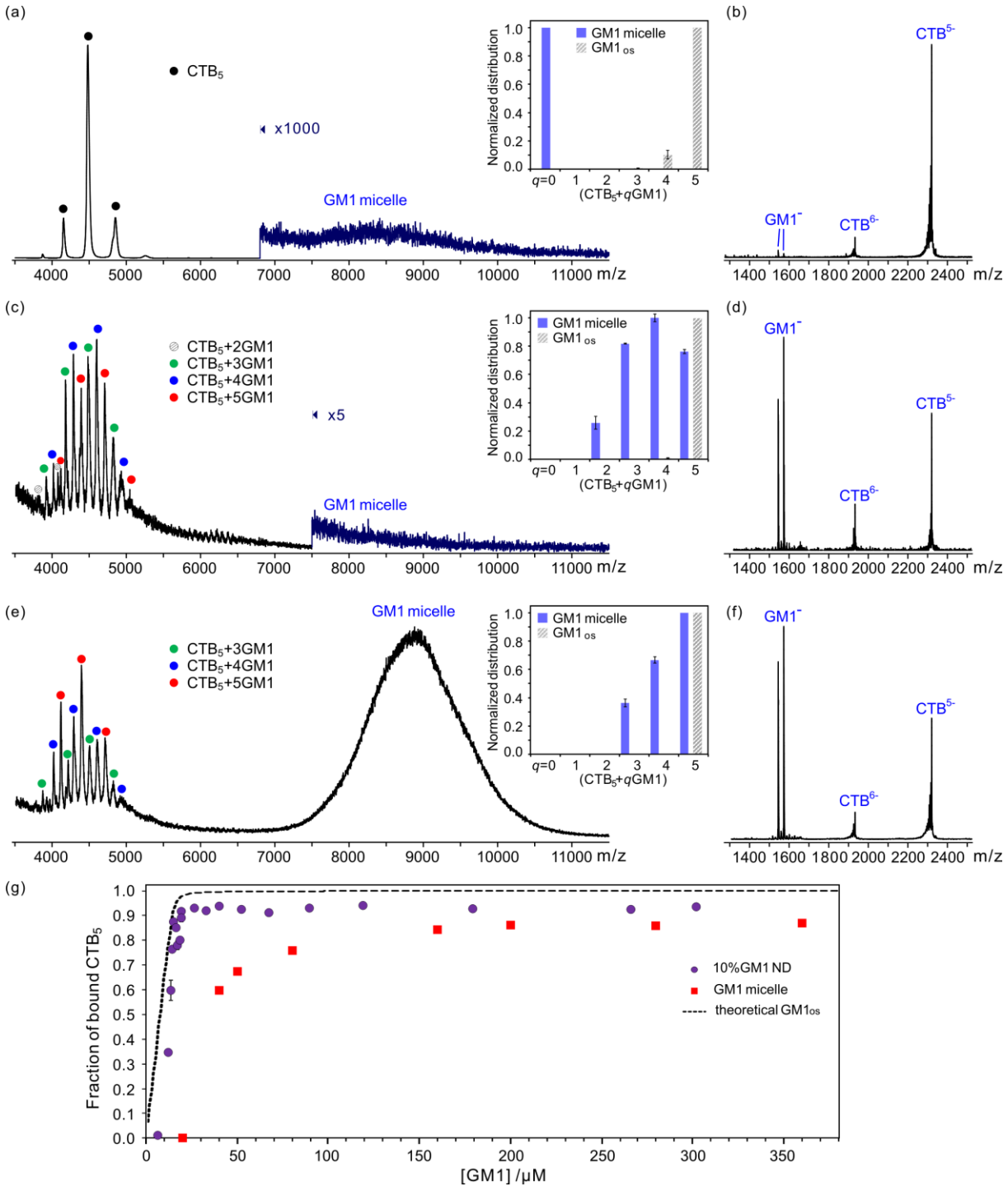
(a)
CTB5
x1000
GM1 micelle
Normalized distribution
GM1 micelle
GM1 os
q=0 1 2 3 4 5
(CTB5+qGM1)
4000 5000 6000 7000 8000 9000 10000 11000 m/z
(b)
CTB5-
GM1-
CTB6-
1400 1600 1800 2000 2200 2400 m/z
(c)
CTB5+2GM1
CTB5+3GM1
CTB5+4GM1
CTB5+5GM1
x5
GM1 micelle
(d)
(e)
(f)
(g)
Fraction of bound CTB5
10%GM1 ND
GM1 micelle
theoretical GM1os
[GM1] /μM

Figure 2

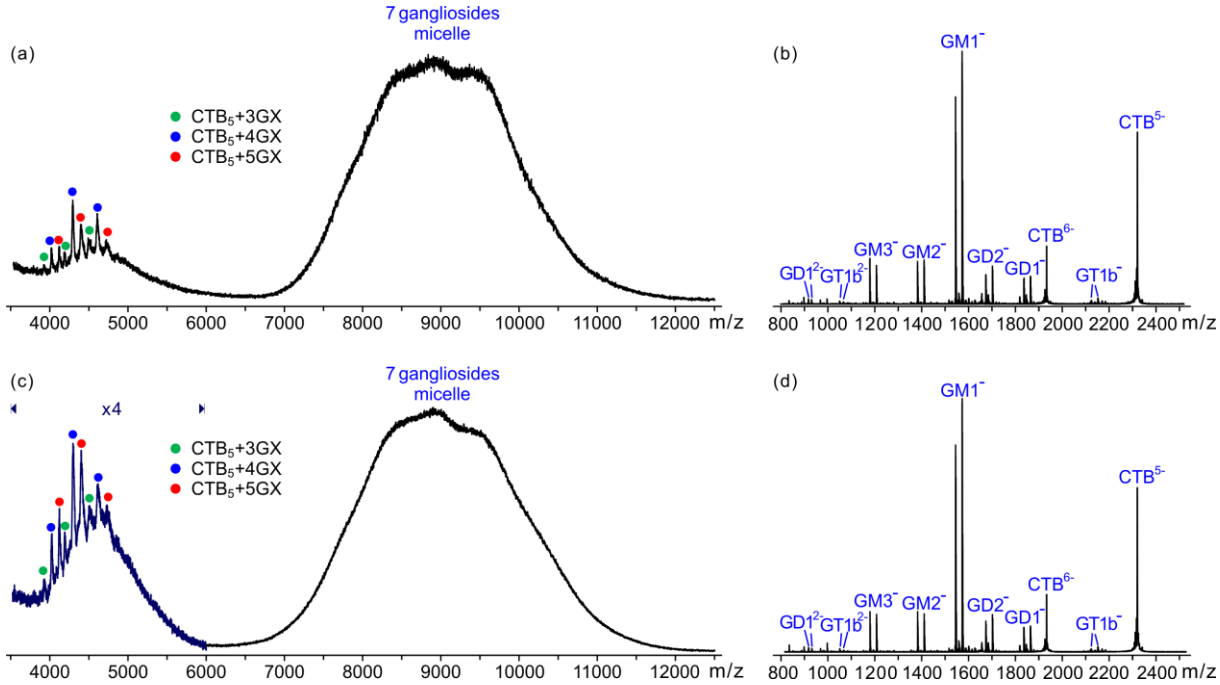
(a)
7 gangliosides micelle
CTB5+3GX
CTB5+4GX
CTB5+5GX
4000 5000 6000 7000 8000 9000 10000 11000 12000 m/z
(b)
GM1-
CTB5-
CTB6-
GM3- GM2-
GD2-
GD1-
GD1 2- GT1b 2-
GT1b-
800 1000 1200 1400 1600 1800 2000 2200 2400 m/z
(c)
x4
7 gangliosides micelle
CTB5+3GX
CTB5+4GX
CTB5+5GX
4000 5000 6000 7000 8000 9000 10000 11000 12000 m/z
(d)
GM1-
CTB5-
CTB6-
GM3- GM2-
GD2-
GD1-
GD1 2- GT1b 2-
GT1b-
800 1000 1200 1400 1600 1800 2000 2200 2400 m/z

Figure 3

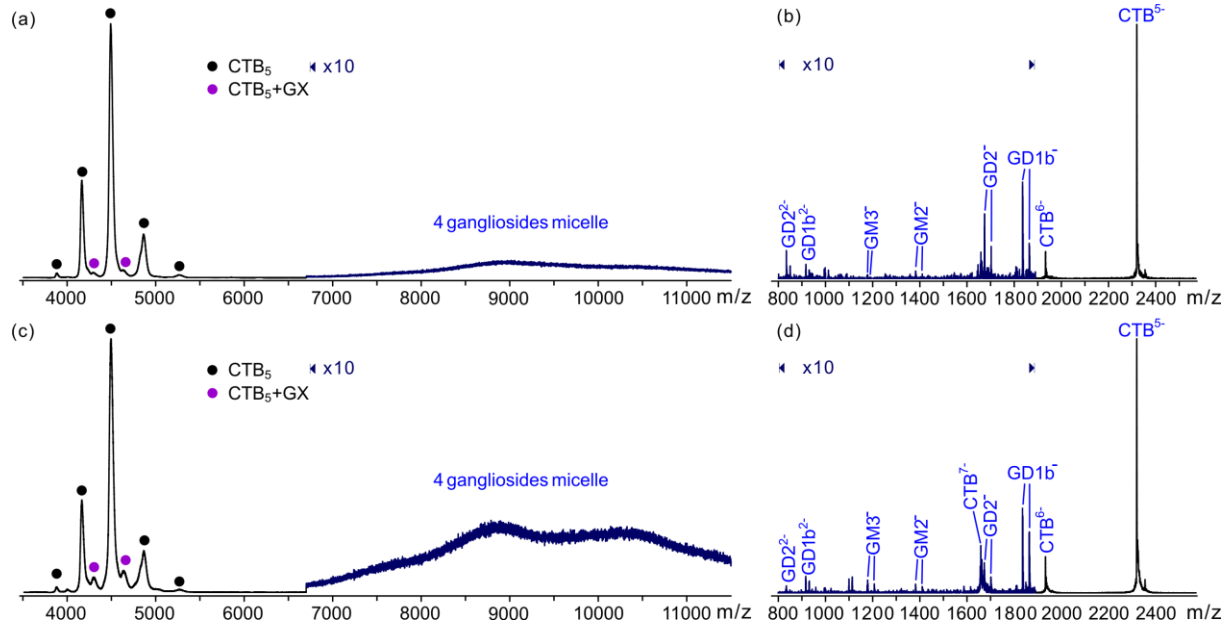
(a)
CTB5
CTB5+GX
x10
4 gangliosides micelle
4000 5000 6000 7000 8000 9000 10000 11000 m/z
(b)
CTB5-
x10
GD2-
GD1b-
GM3-
GM2-
GD2-
GD1b-
CTB6-
800 1000 1200 1400 1600 1800 2000 2200 2400 m/z
(c)
CTB5
CTB5+GX
x10
4 gangliosides micelle
4000 5000 6000 7000 8000 9000 10000 11000 m/z
(d)
CTB5-
x10
GD2-
GD1b-
GM3-
GM2-
CTB7-
GD2-
GD1b-
CTB6-
800 1000 1200 1400 1600 1800 2000 2200 2400 m/z

Figure 4

SUPPORTING INFORMATION FOR:

Detecting Protein-Glycolipid Interactions using Glycomicelles and CaR-ESI-MS

Ling Han, Elena N. Kitova and John S. Klassen

Table S1. List of the theoretical and experimental m/z values for free and ganglioside-bound CTB_5 and $Stx1B_5$ ions.

	Theoretical m/z [a]				Experimental m/z [b]			
Charge state	-14	-13	-12		-14	-13	-12	
CTB_5	4145	4464	4836		4152 ± 7	4482 ± 10	4855 ± 10	
CTB_5+GD1a	4277	4606	4990		4282 ± 9	4618 ± 9	5007 ± 7	
CTB_5+GD1b	4277	4606	4990		4289 ± 4	4629 ± 7	5008 ± 6	
CTB_5+GT1b	4297	4628	5014		4304 ± 6	4642 ± 9	5026 ± 4	
CTB_5+GD2	4265	4593	4976		4283 ± 6	4613 ± 7	4999 ± 8	
Charge state	-16	-15	-14	-13	-16	-15	-14	-13
CTB_5+2GM1	3821	4076	4367	4703	3824 ± 3	4079 ± 2	ND [c]	ND [c]
CTB_5+3GM1	3919	4180	4479	4823	3923 ± 2	4184 ± 2	4494 ± 10	4826 ± 4
CTB_5+4GM1	4016	4284	4590	4943	4020 ± 2	4290 ± 3	4603 ± 4	4949 ± 4
CTB_5+5GM1	4114	4388	4701	5063	4120 ± 1	4391 ± 8	4713 ± 3	5065 ± 5
Charge state	-11	-10	-9		-11	-10	-9	
$Stx1B_5$	3495	3844	4272		3506 ± 4	3863 ± 4	4293 ± 8	
$Stx1B_5$+GD1a	3663	4029	4477		3681 ± 1	4046 ± 2	4500 ± 9	
$Stx1B_5$+GD1b	3663	4029	4477		3674 ± 2	4044 ± 3	4495 ± 5	
$Stx1B_5$+GT1b	3689	4058	4509		3705 ± 1	4076 ± 6	4525 ± 6	
$Stx1B_5$+GD2	3648	4013	4459		3656 ± 3	4020 ± 3	4475 ± 4	

a. The average MWs of the two major isoforms (d18:1-18:0 and d20:1-18:0) of each ganglioside were used to calculate the theoretical m/z values. b. The errors correspond to one standard deviation. c. ND = not detected.

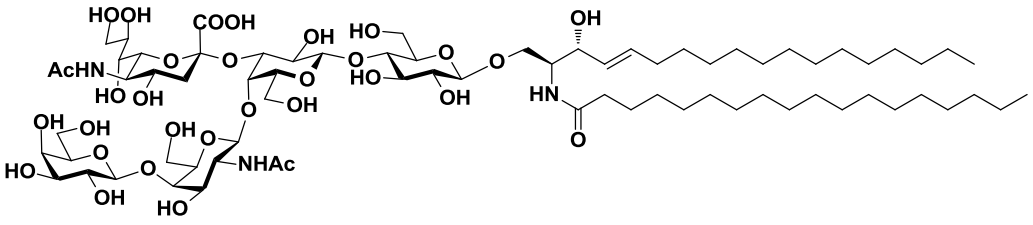

GM1 (*d*18:1-18:0) MW 1545.88 Da

β-D-Gal-(1,3)-β-D-GalNAc-(1,4)-[α-D-Neu5Ac-(2,3)]-β-D-Gal-(1,4)-β-D-Glc-ceramide

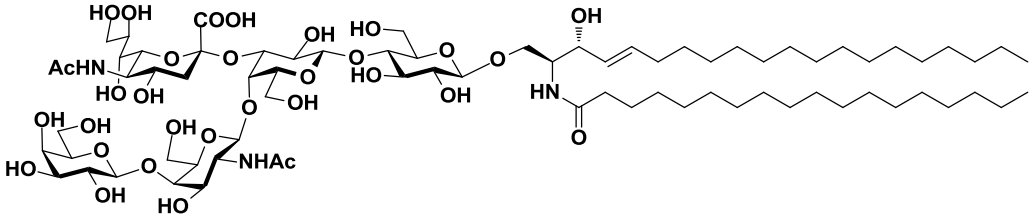

GM1 (*d*20:1-18:0) MW 1573.91 Da

β-D-Gal-(1,3)-β-D-GalNAc-(1,4)-[α-D-Neu5Ac-(2,3)]-β-D-Gal-(1,4)-β-D-Glc-ceramide

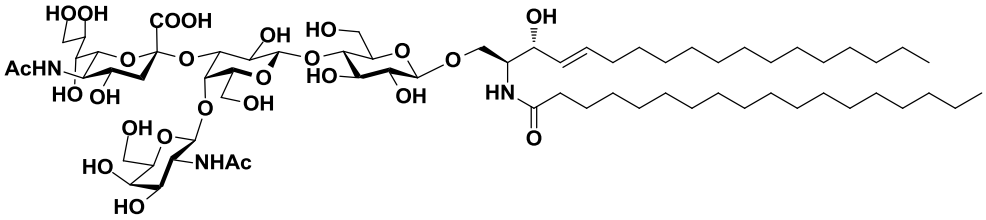

GM2 (*d*18:1-18:0) MW 1383.82 Da

β-D-GalNAc-(1,4)-[α-D-Neu5Ac-(2,3)]-β-D-Gal-(1,4)-β-D-Glc-ceramide

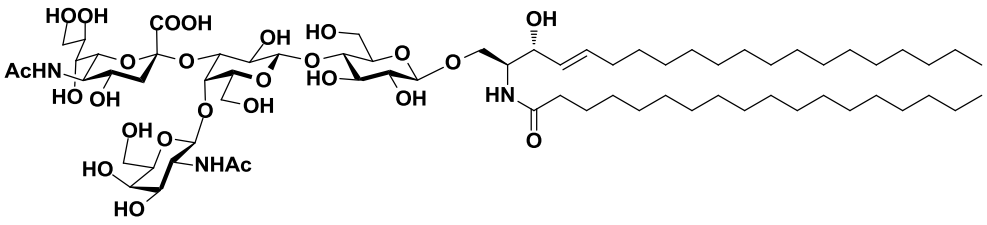

GM2 (*d*20:1-18:0) MW 1411.86 Da

β-D-GalNAc-(1,4)-[α-D-Neu5Ac-(2,3)]-β-D-Gal-(1,4)-β-D-Glc-ceramide

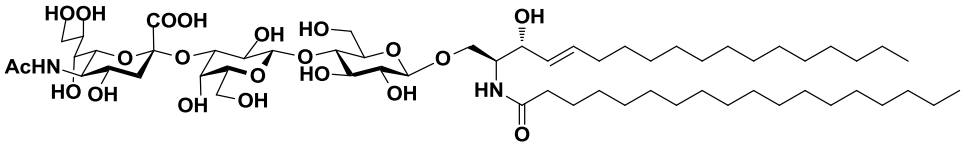

GM3 (*d*18:1-18:0) MW 1180.74 Da

α-D-Neu5Ac-(2,3)-β-D-Gal-(1,4)-β-D-Glc-ceramide

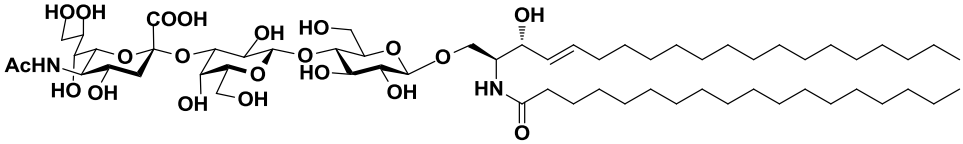

GM3 (*d*20:1-18:0) MW 1208.78 Da

α-D-Neu5Ac-(2,3)-β-D-Gal-(1,4)-β-D-Glc-ceramide

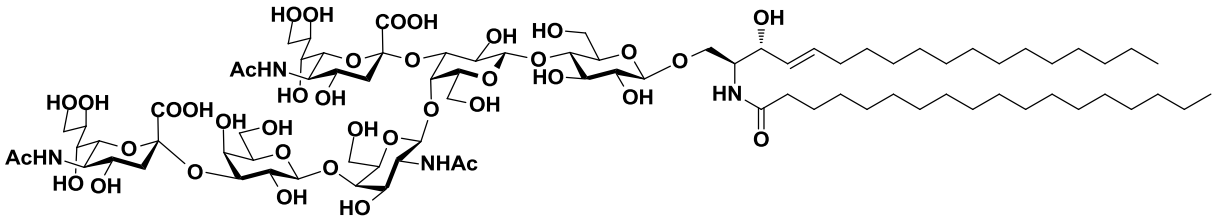

GD1a (*d*18:1-18:0) MW 1836.97 Da

α-D-Neu5Ac-(2,3)-β-D-Gal-(1,3)-β-D-GalNAc-(1,4)-[α-D-Neu5Ac-(2,3)]-β-D-Gal-(1,4)-

β-D-Glc-ceramide

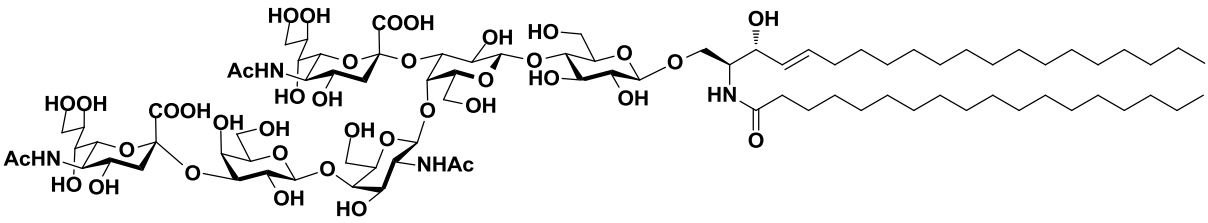

GD1a (*d*20:1-18:0) MW 1865.00 Da

α-D-Neu5Ac-(2,3)-β-D-Gal-(1,3)-β-D-GalNAc-(1,4)-[α-D-Neu5Ac-(2,3)]-β-D-Gal-(1,4)-β-D-Glc-ceramide

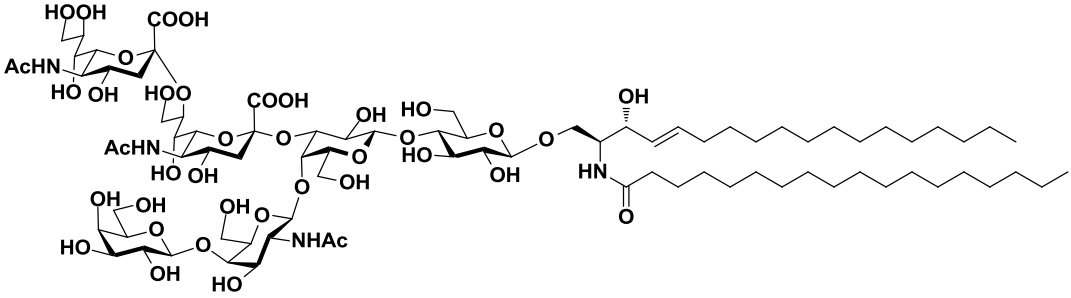

GD1b (*d*18:1-18:0) MW 1836.97 Da

β-D-Gal-(1,3)-β-D-GalNAc-(1,4)-[α-D-Neu5Ac-(2,8)-α-D-Neu5Ac-(2,3)]-β-D-Gal-(1,4)-β-D-Glc-ceramide

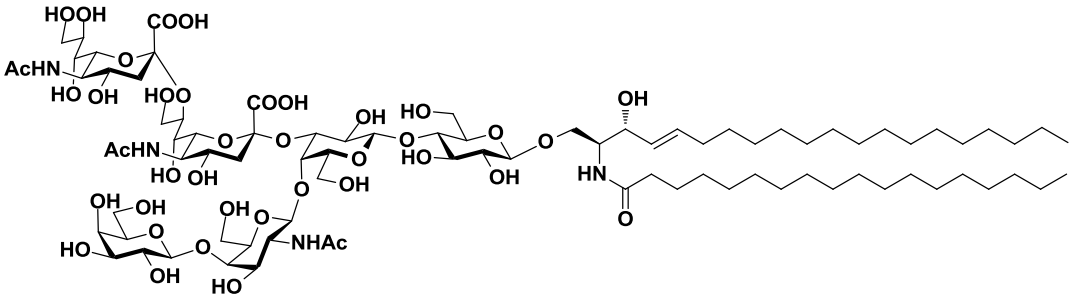

GD1b (*d*20:1-18:0) MW 1865.00 Da

β-D-Gal-(1,3)-β-D-GalNAc-(1,4)-[α-D-Neu5Ac-(2,8)-α-D-Neu5Ac-(2,3)]-β-D-Gal-(1,4)-β-D-Glc-ceramide

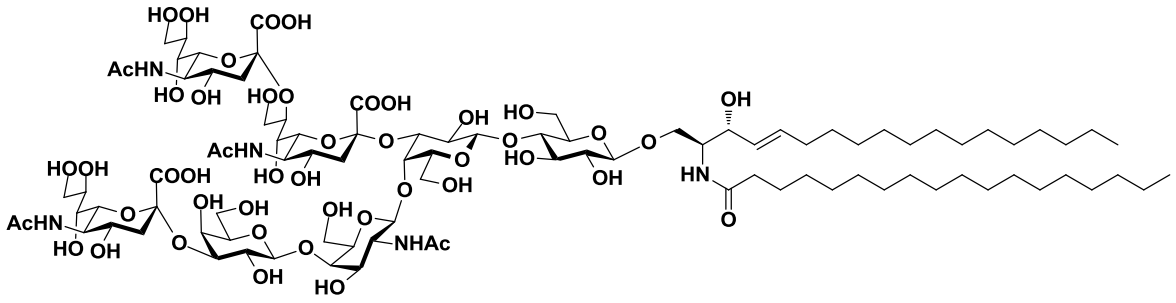

GT1b (*d*18:1-18:0) MW 2128.07 Da

α-D-Neu5Ac-(2,3)-β-D-Gal-(1,3)-β-D-GalNAc-(1,4)-[α-D-Neu5Ac-(2,8)-α-D-Neu5Ac-(2,3)]-β-D-Gal-(1,4)-β-D-Glc-ceramide

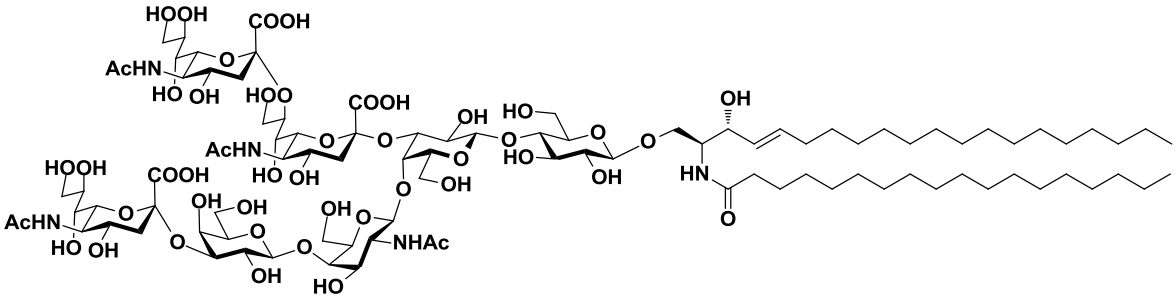

GT1b (*d*20:1-18:0) MW 2156.10 Da

α-D-Neu5Ac-(2,3)-β-D-Gal-(1,3)-β-D-GalNAc-(1,4)-[α-D-Neu5Ac-(2,8)-α-D-Neu5Ac-(2,3)]-β-D-Gal-(1,4)-β-D-Glc-ceramide

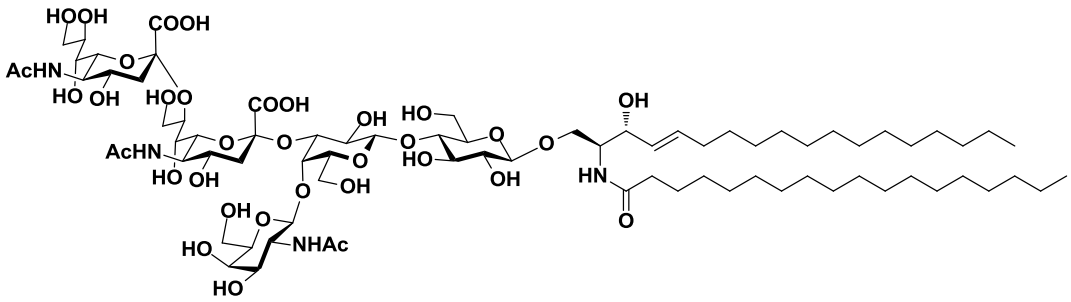

GD2 (*d*18:1-18:0) MW 1674.92 Da

β-D-GalNAc-(1,4)-[α-D-Neu5Ac-(2,8)-α-D-Neu5Ac-(2,3)]-β-D-Gal-(1,4)-β-D-Glc-ceramide

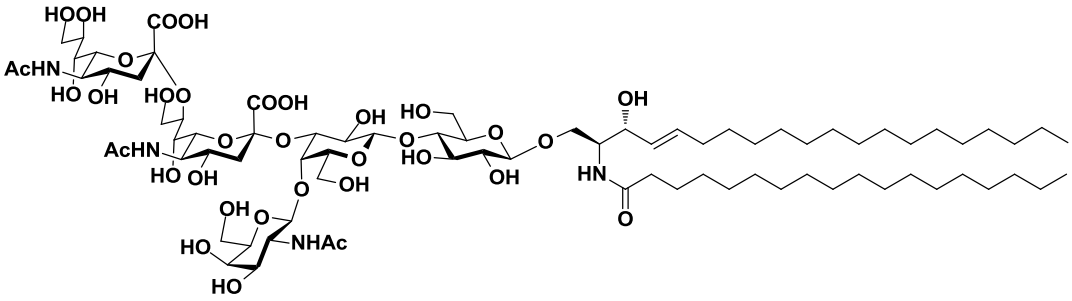

GD2 (*d*20:1-18:0) MW 1702.95 Da

β-D-GalNAc-(1,4)-[α-D-Neu5Ac-(2,8)-α-D-Neu5Ac-(2,3)]-β-D-Gal-(1,4)-β-D-Glc-ceramide

Figure S1. Structures of the gangliosides GM1, GM2, GM3, GD1a, GD1b, GT1b and GD2. For each ganglioside, the two major isoforms (*d*18:1-18:0 and *d*20:1-18:0) are shown.

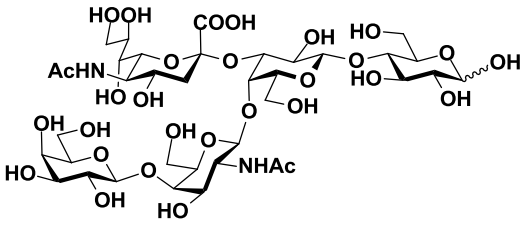

$GM1_{os}$ MW 998.34 Da

β-D-Gal-(1,3)-β-D-GalNAc-(1,4)-[α-D-Neu5Ac-(2,3)]-β-D-Gal-(1,4)-D-Glc

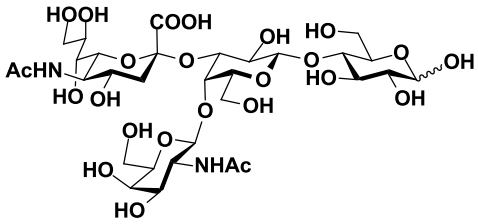

$GM2_{os}$ MW 836.29 Da

β-D-GalNAc-(1,4)-[α-D-Neu5Ac-(2,3)]-β-D-Gal-(1,4)-D-Glc

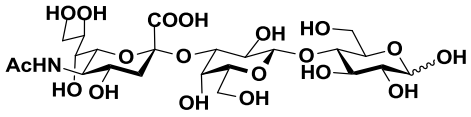

$GM3_{os}$ MW 633.21 Da

α-D-Neu5Ac-(2,3)-β-D-Gal-(1,4)-D-Glc

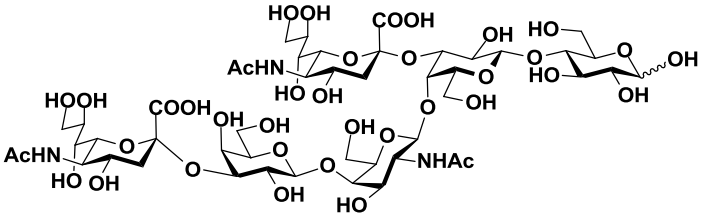

$GD1a_{os}$ MW 1289.44 Da

α-D-Neu5Ac-(2,3)-β-D-Gal-(1,3)-β-D-GalNAc-(1,4)-[α-D-Neu5Ac-(2,3)]-β-D-Gal-(1,4)-D-Glc

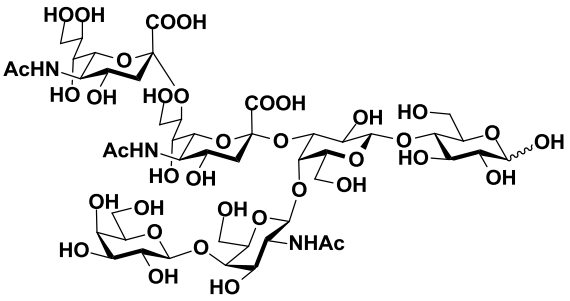

GD1b$_{os}$ MW 1289.44 Da

β-D-Gal-(1,3)-β-D-GalNAc-(1,4)-[α-D-Neu5Ac-(2,8)-α-D-Neu5Ac-(2,3)]-β-D-Gal-(1,4)-D-Glc

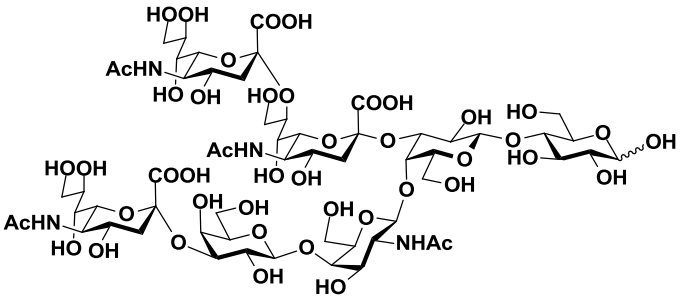

GT1b$_{os}$ MW 1580.53 Da

α-D-Neu5Ac-(2,3)-β-D-Gal-(1,3)-β-D-GalNAc-(1,4)-[α-D-Neu5Ac-(2,8)-α-D-Neu5Ac-(2,3)]-

β-D-Gal-(1,4)-D-Glc

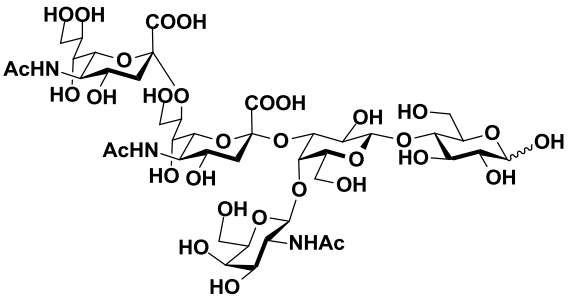

GD2$_{os}$ MW 1127.39 Da

β-D-GalNAc-(1,4)-[α-D-Neu5Ac-(2,8)-α-D-Neu5Ac-(2,3)]-β-D-Gal-(1,4)-D-Glc

Figure S2. Structures of the ganglioside oligosaccharides $GM1_{os}$, $GM2_{os}$, $GM3_{os}$, $GD1a_{os}$, $GD1b_{os}$, $GT1b_{os}$ and $GD2_{os}$.

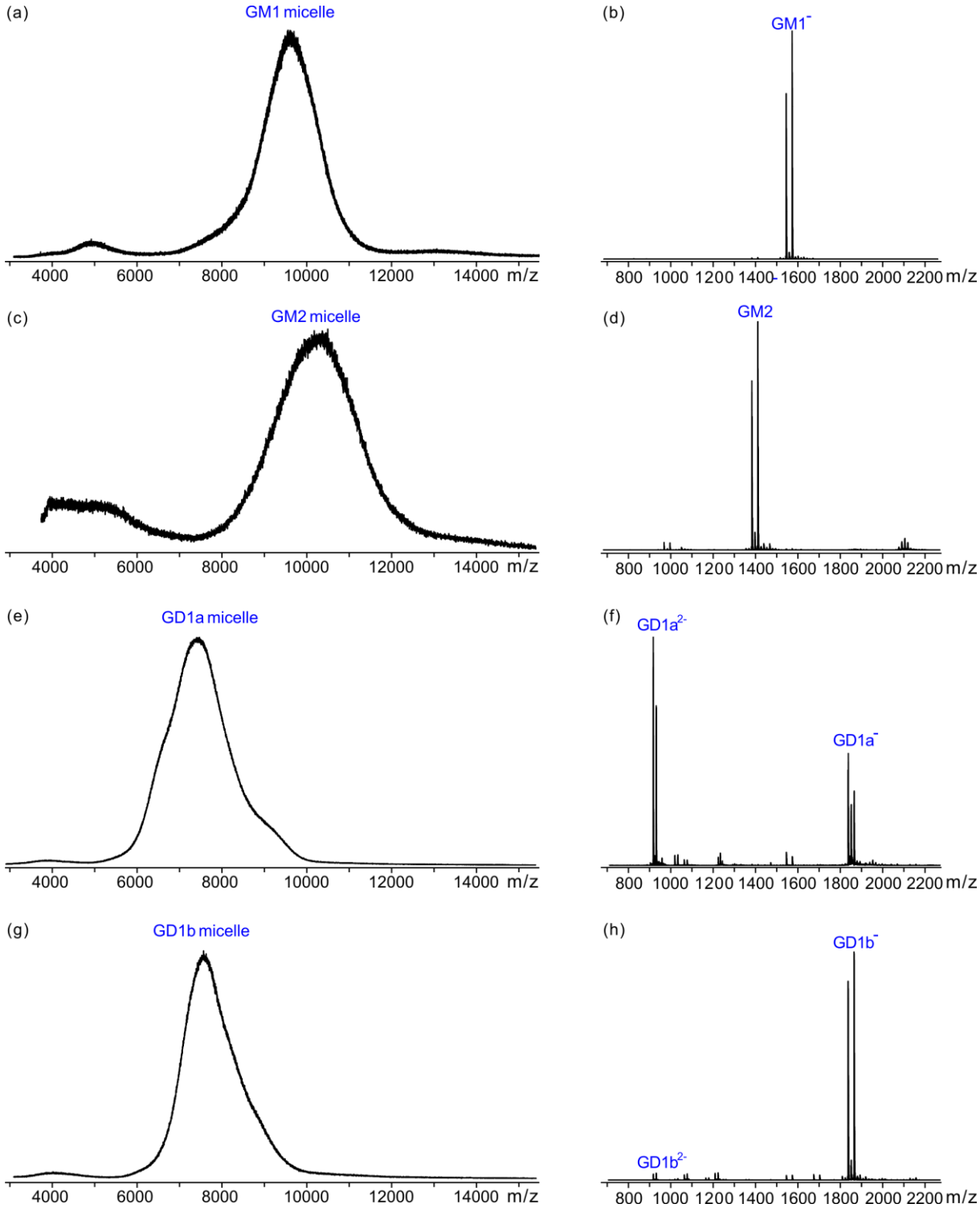
(a)
GM1 micelle
4000 6000 8000 10000 12000 14000 m/z
(b)
GM1-
800 1000 1200 1400 1600 1800 2000 2200 m/z
(c)
GM2 micelle
4000 6000 8000 10000 12000 14000 m/z
(d)
GM2
800 1000 1200 1400 1600 1800 2000 2200 m/z
(e)
GD1a micelle
4000 6000 8000 10000 12000 14000 m/z
(f)
GD1a2-
GD1a-
800 1000 1200 1400 1600 1800 2000 2200 m/z
(g)
GD1b micelle
4000 6000 8000 10000 12000 14000 m/z
(h)
GD1b-
GD1b2-
800 1000 1200 1400 1600 1800 2000 2200 m/z

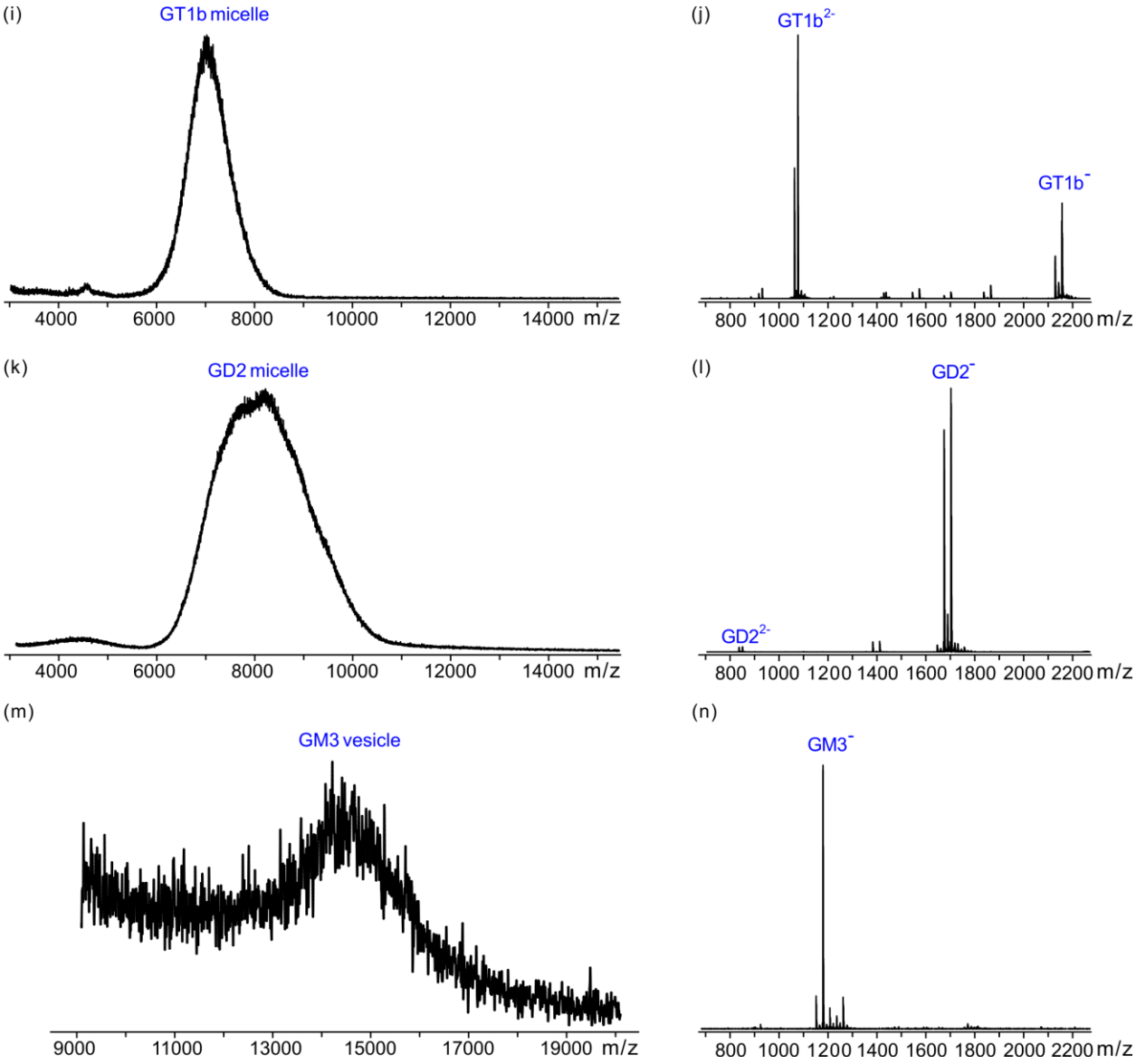

Figure S3. ESI mass spectra acquired in negative ion mode for aqueous ammonium acetate solutions (200 mM, 25 °C and pH 6.8) of 400 μM (a) GM1, (c) GM2, (e) GD1a, (g) GD1b, (i) GT1b, (k) GD2, and (m) GM3. (b), (d), (f), (h), (j), (l) and (n) CID mass spectra measured for ions produced by ESI from the solutions described in (a), (c), (e), (g), (i), (k) and (m), respectively. A ~200 m/z isolation window, centered at (b) m/z 9,000, (d) m/z 10,000, (f) m/z 8,000, (h) m/z 8,000, (j) m/z 7,000, (l) m/z 8,000 and (n) m/z 15,000 was used. CID was performed in the Trap using a collision energy of 100 V.

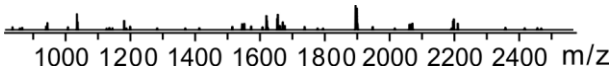

Figure S4. CID mass spectrum acquired in negative ion mode for an aqueous ammonium acetate solutions (200 mM, 25 °C and pH 6.8) of 400 µM GM1. Ions within a window of m/z values (~50 m/z units wide) centred at m/z 4,400 were isolated and subjected to CID in the Trap using a collision energy of 100 V.

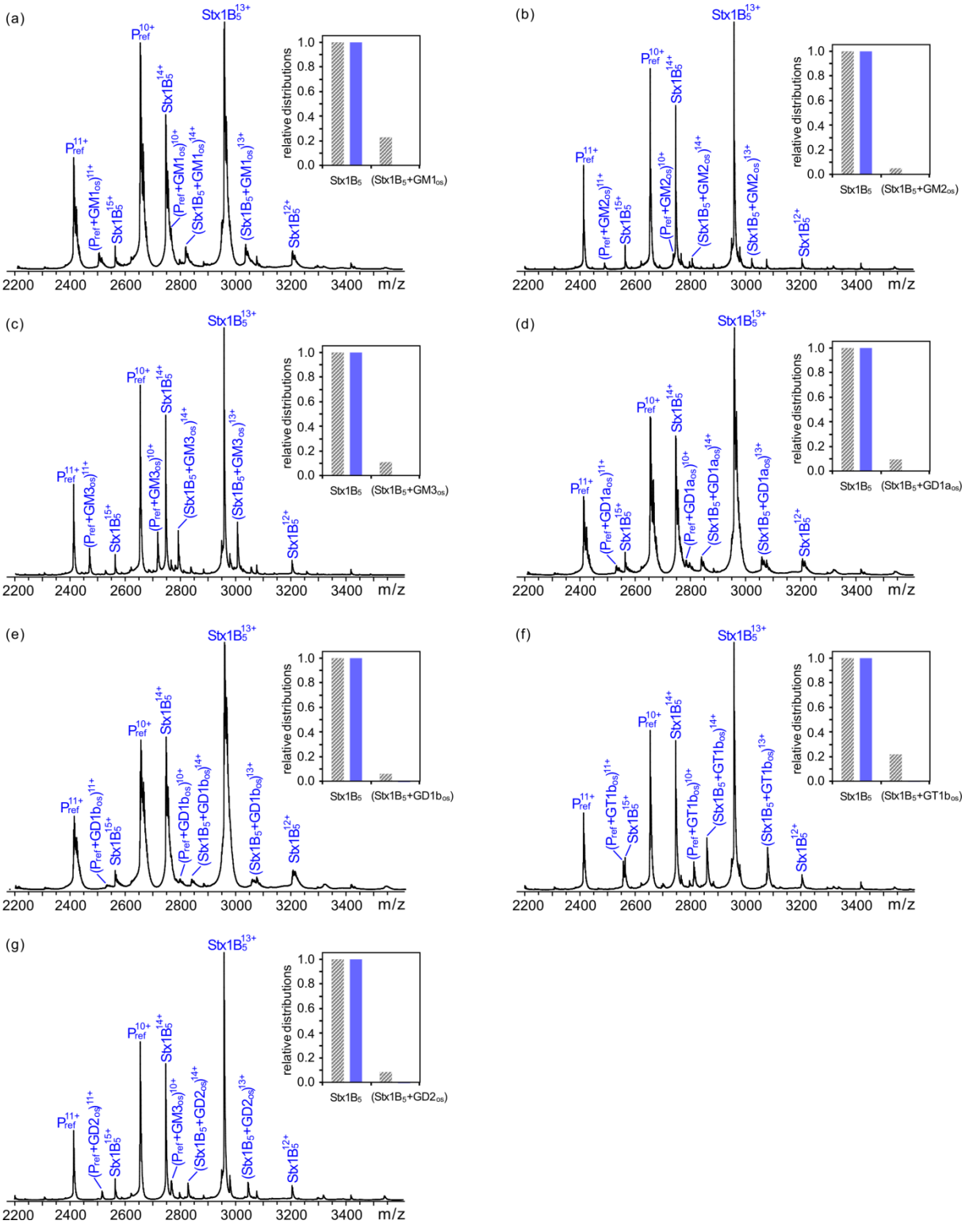
(a)
(b)
(c)
(d)
(e)
(f)
(g)
relative distributions
m/z

Figure S5. ESI mass spectra acquired in positive ion mode for aqueous ammonium acetate solutions (200 mM, 25 °C and pH 6.8) of $Stx1B_5$ (3.0 μM) with 100 μM (a) $GM1_{os}$; (b) $GM2_{os}$; (c) $GM3_{os}$; (d) $GD1a_{os}$; (e) $GD1b_{os}$; (f) $GT1b_{os}$; and (g) $GD2_{os}$. scFv (2.0 μM), which served as P_{ref}, was added into each solution to correct for the nonspecific ligand binding during the ESI process [S1,S2]. Insets show the normalized distributions of free and oligosaccharide-bound $Stx1B_5$ measured from mass spectrum before (▨) and after (■) correction for the nonspecific binding.

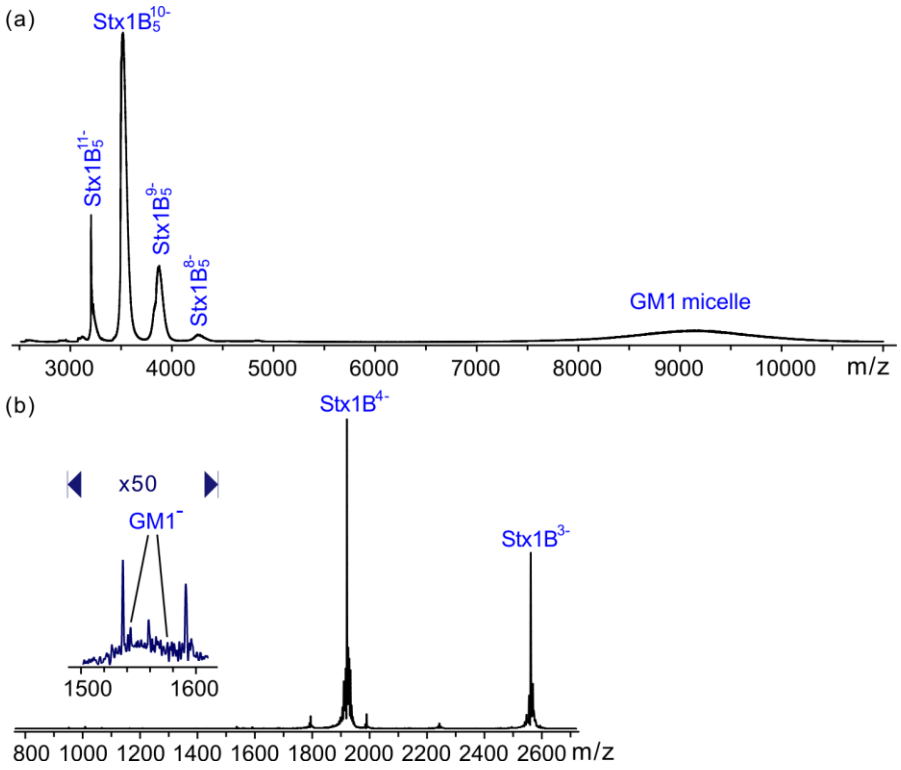

Figure S6. (a) ESI mass spectrum acquired in negative ion mode for an aqueous ammonium acetate solution (200 mM, 25 °C and pH 6.8) of $Stx1B_5$ (3 µM) with 320 µM GM1. (b) CID mass spectrum measured for ions produced by ESI from the solution described in (a). Ions within a window of m/z values (~50 m/z units wide) centred at m/z 3,660 (which corresponds to the -11 charge state of $Stx1B_5$ bound to GM1) were isolated and subjected to CID in the Trap using a collision energy of 100 V.

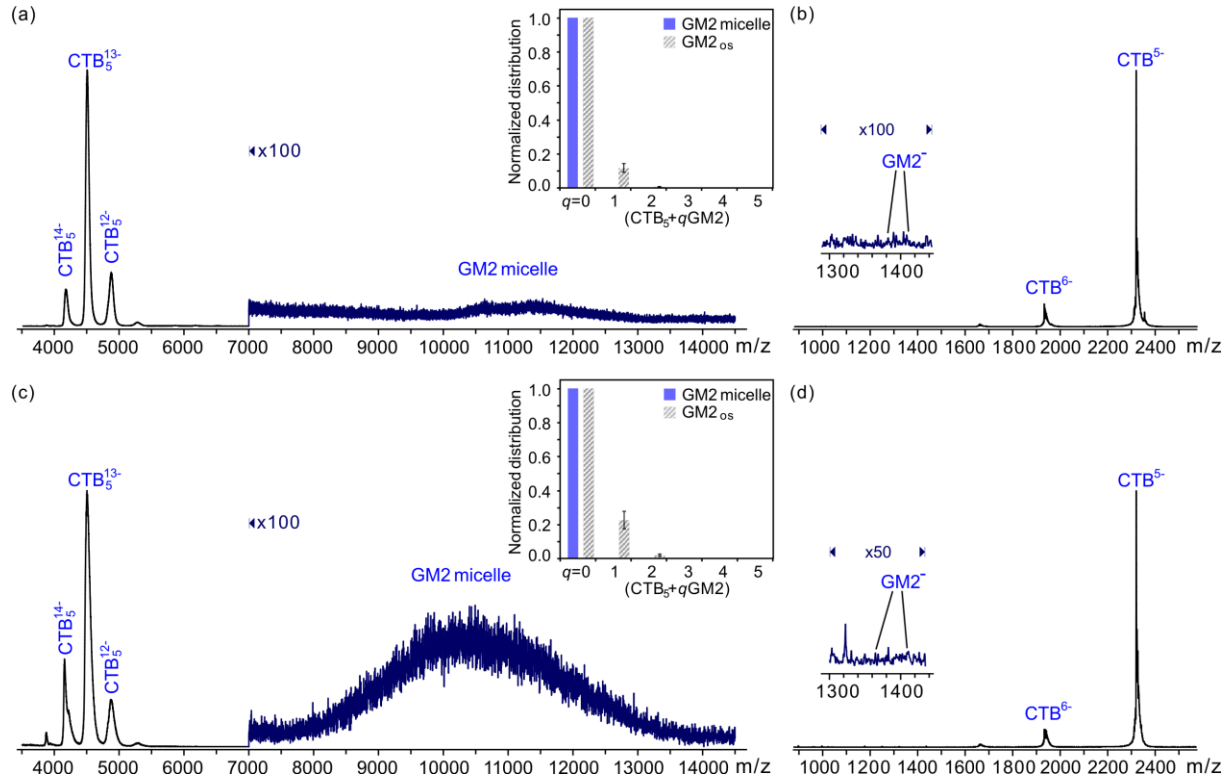

Figure S7. ESI mass spectra acquired in negative ion mode for aqueous ammonium acetate solutions (200 mM, 25 °C and pH 6.8) of CTB_5 (3 μM) with GM2 at concentrations of (a) 200 μM and (c) 360 μM. Insets show the normalized distributions of free and GM2-bound CTB_5. Also shown are the distributions of bound $GM2_{os}$ expected based on the association constants reported in reference S3; the errors were calculated from propagation of uncertainties in the reported association constants. (b) and (d) CID mass spectra measured for ions produced by ESI for the solutions described in (a) and (c), respectively. Ions within a window of m/z values (~50 m/z units wide) centred at 4,575 (which corresponds to the -13 charge state of CTB_5 bound to GM2) were isolated and subjected to CID in the Trap using a collision energy of 100 V.

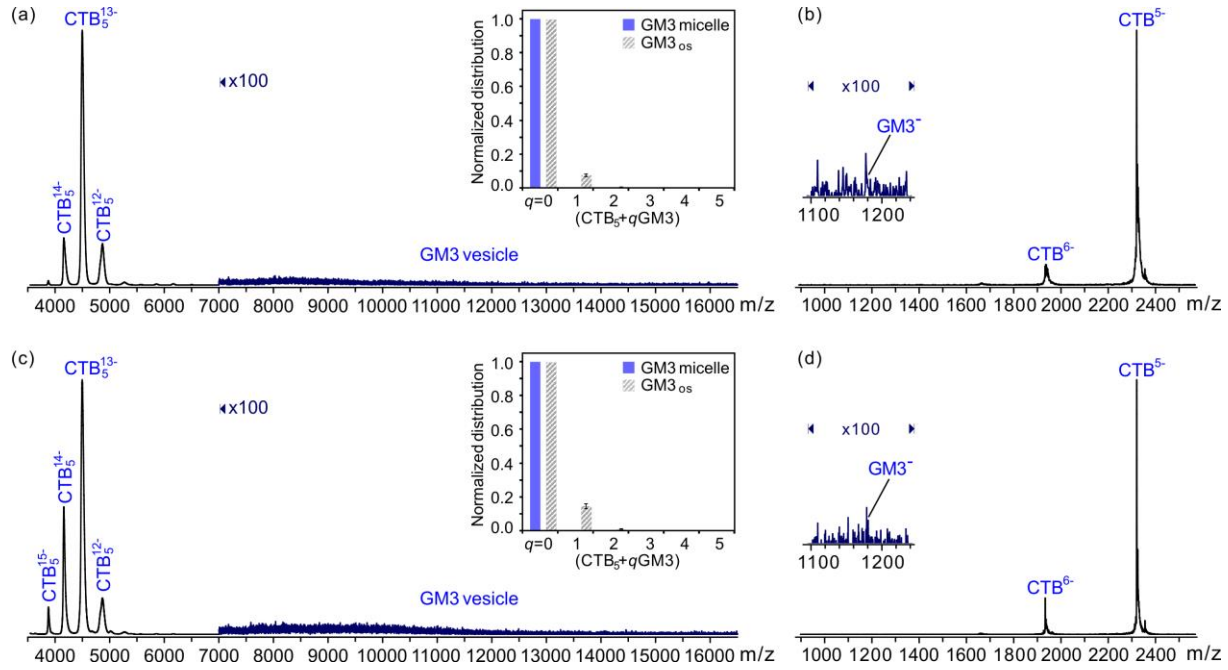

Figure S8. ESI mass spectra acquired in negative ion mode for aqueous ammonium acetate solutions (200 mM, 25 °C and pH 6.8) of CTB_5 (3 μM) with GM3 at concentrations of (a) 200 μM and (c) 360 μM. Insets show the normalized distributions of free and GM3-bound CTB_5. Also shown are the distributions of bound $GM3_{os}$ expected based on the association constants reported in reference S3; the errors were calculated from propagation of uncertainties in the reported association constants. (b) and (d) CID mass spectra measured for ions produced by ESI for the solutions described in (a) and (c), respectively. Ions within a window of m/z values (~50 m/z units wide) centred at m/z 4,565 (which corresponds to the -13 charge state of CTB_5 bound to GM3) were isolated and subjected to CID in the Trap using a collision energy of 100 V.

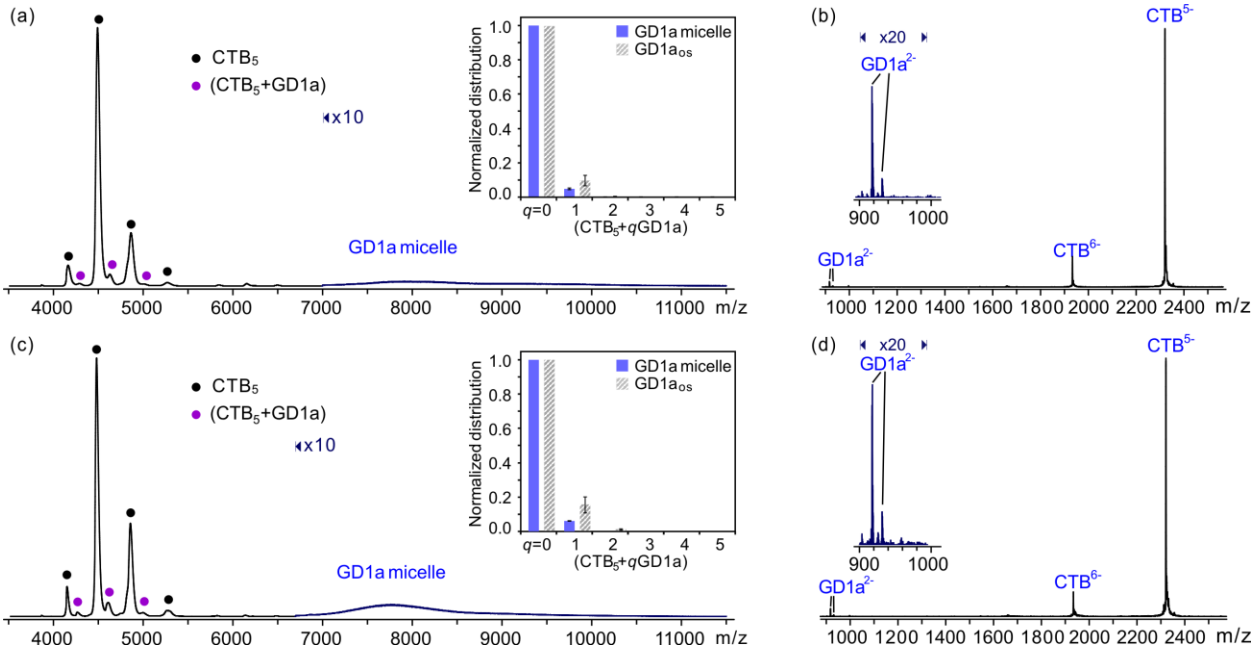

Figure S9. ESI mass spectra acquired in negative ion mode for aqueous ammonium acetate solutions (200 mM, 25 °C and pH 6.8) of CTB_5 (3 µM) with GD1a at concentrations of (a) 200 µM and (c) 360 µM. Insets show the normalized distributions of free and GD1a-bound CTB_5; the reported errors correspond to one standard deviation. Also shown are the distributions of bound $GD1a_{os}$ expected based on the association constants reported in reference S3; the errors were calculated from propagation of uncertainties in the reported association constants. (b) and (d) CID mass spectra measured for ions produced by ESI for the solutions described in (a) and (c), respectively. Ions within a window of m/z values (~50 m/z units wide) centred at m/z 4,610 (which corresponds to the -13 charge state of CTB_5 bound to GD1a) were isolated and subjected to CID in the Trap using a collision energy of 100 V.

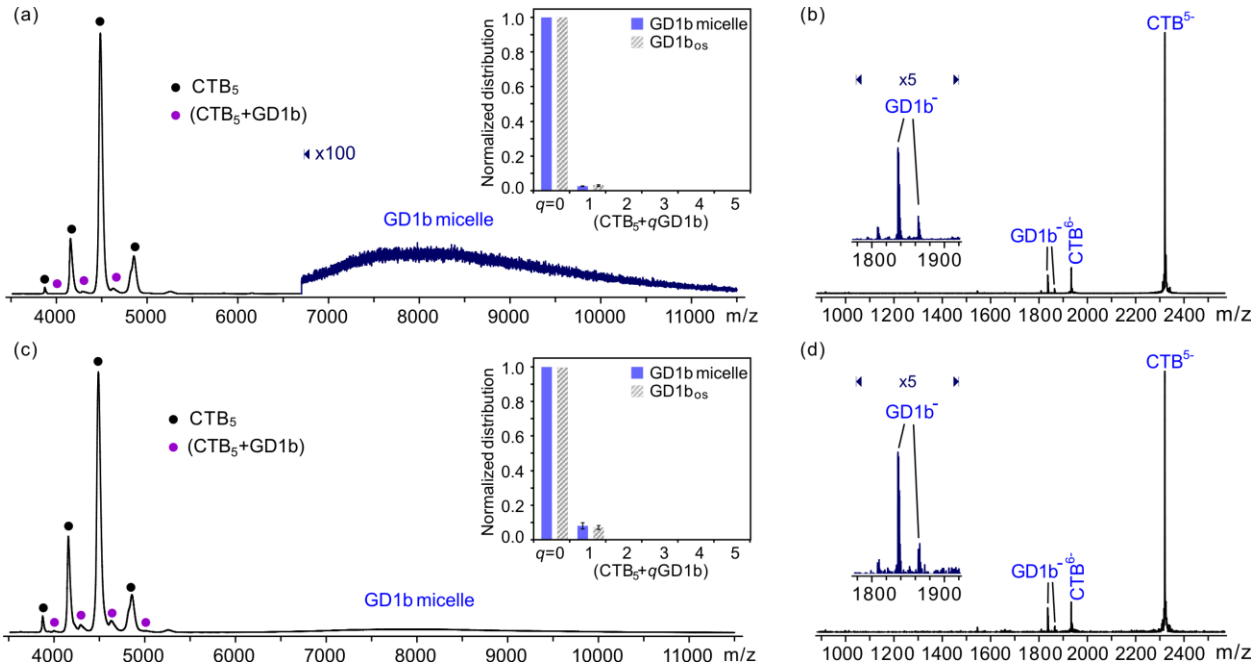

Figure S10. ESI mass spectra acquired in negative ion mode for aqueous ammonium acetate solutions (200 mM, 25 °C and pH 6.8) of CTB_5 (3 µM) with GD1b at concentrations of (a) 80 µM and (c) 200 µM. Insets show the normalized distributions of free and GD1b-bound CTB_5; the reported errors correspond to one standard deviation. Also shown are the distributions of bound $GD1b_{os}$ expected based on the association constants reported in reference S3; the errors were calculated from propagation of uncertainties in the reported association constants. (b) and (d) CID mass spectra measured for ions produced by ESI for the solutions described in (a) and (c), respectively. Ions within a window of m/z values (~50 m/z units wide) centred at m/z 4,610 (which corresponds to the -13 charge state of CTB_5 bound to GD1b) were isolated and subjected to CID in the Trap using a collision energy of 100 V.

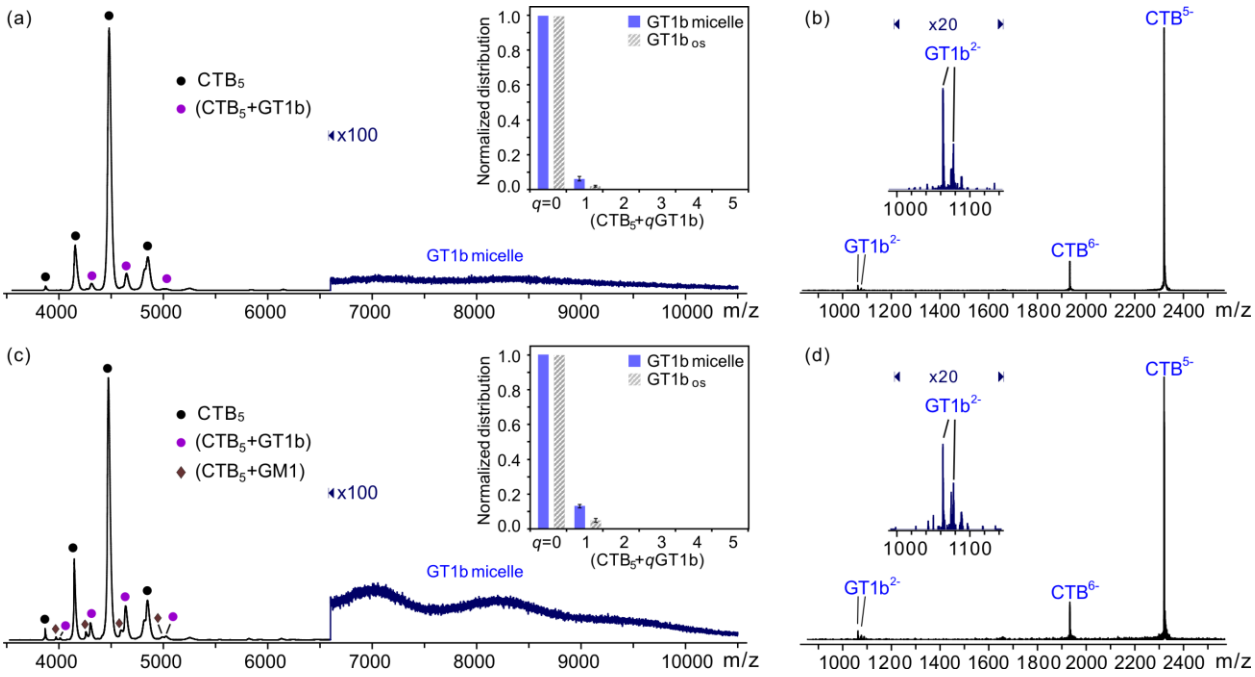

Figure S11. ESI mass spectra acquired in negative ion mode for aqueous ammonium acetate solutions (200 mM, 25 °C and pH 6.8) of CTB_5 (3 μM) with GT1b at concentrations of (a) 80 μM and (c) 200 μM. Insets show the normalized distributions of free and GT1b-bound CTB_5; the reported errors correspond to one standard deviation. Also shown are the distributions of bound $GT1b_{os}$ expected based on the association constants reported in reference S3; the errors were calculated from propagation of uncertainties in the reported association constants. The signal corresponding to GM1-bound CTB_5 observed in (c) is attributed to the presence of trace GM1 impurity in the GT1b sample. (b) and (d) CID mass spectra measured for ions produced by ESI for the solutions described in (a) and (c), respectively. Ions within a window of m/z values (~50 m/z units wide) centred at m/z 4,631 (which corresponds to the -13 charge state of CTB_5 bound to GT1b) were isolated and subjected to CID in the Trap using a collision energy of 100 V.

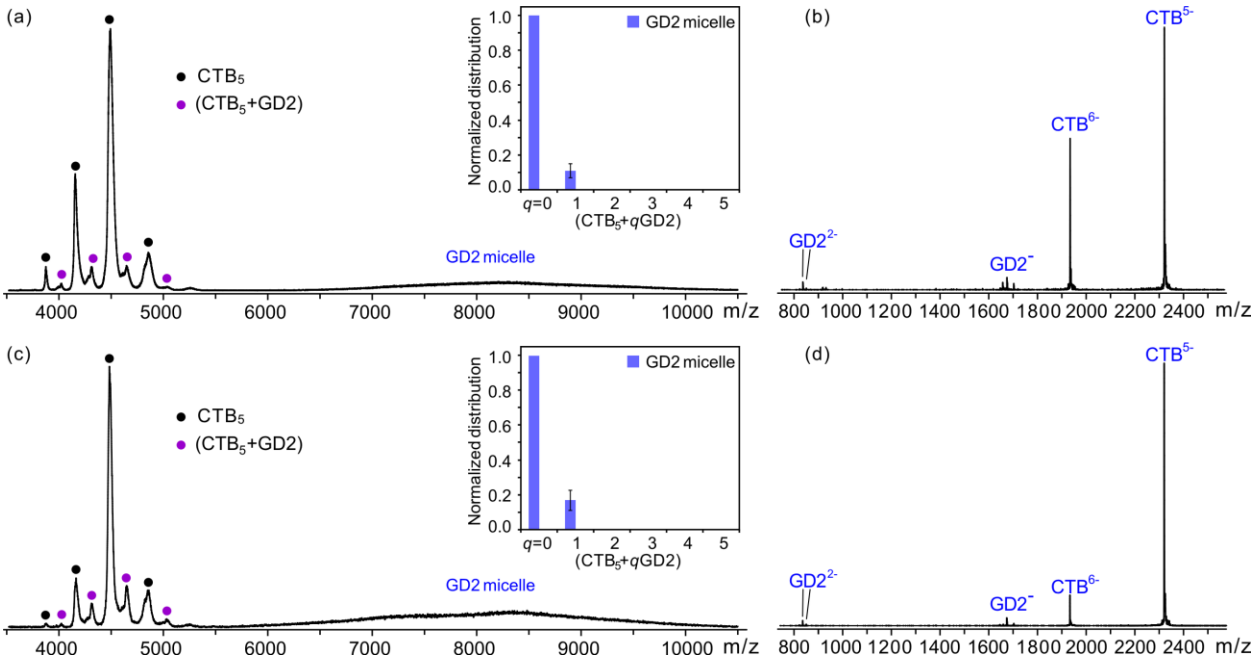

Figure S12. ESI mass spectra acquired in negative ion mode for aqueous ammonium acetate solutions (200 mM, 25 °C and pH 6.8) of CTB_5 (3 µM) with GD2 at concentrations of (a) 80 µM and (c) 200 µM. Insets show the normalized distributions of free and GD2-bound CTB_5; the reported errors correspond to one standard deviation. (b) and (d) CID mass spectra measured for ions produced by ESI for the solutions described in (a) and (c), respectively. Ions within a window of m/z values (~50 m/z units wide) centred at m/z 4,600 (which corresponds to the -13 charge state of CTB_5 bound to GD2) were isolated and subjected to CID in the Trap using a collision energy of 100 V.

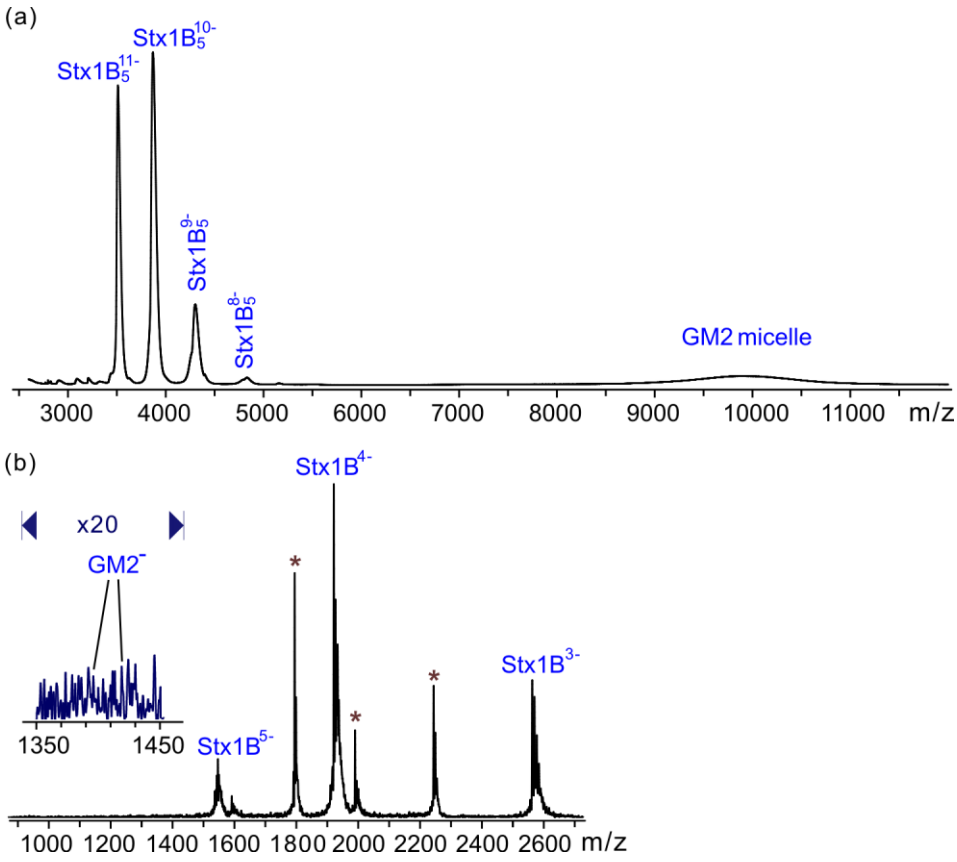

Figure S13. (a) ESI mass spectrum (acquired in negative ion mode for aqueous ammonium acetate solution (200 mM, 25 °C and pH 6.8) of $Stx1B_5$ (3 µM) with 320 µM GM2. (b) CID mass spectrum measured for ions produced by ESI for the solutions described in (a). Ions within a window of m/z values (~50 m/z units wide) centred at m/z 4,015 (which corresponds to the -10 charge state of $Stx1B_5$ bound to GM2) were isolated and subjected to CID in the Trap using a collision energy of 100 V. Peaks labeled with * correspond to CID fragment ions produced from impurities in $Stx1B_5$ sample.

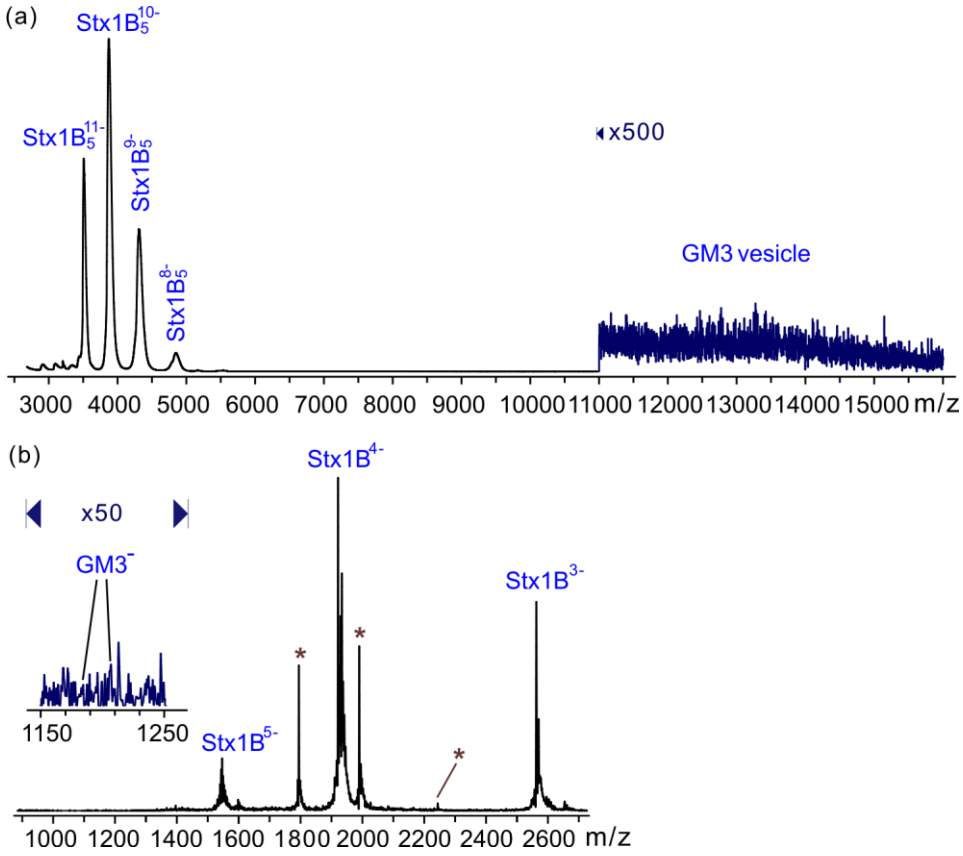

Figure S14. (a) ESI mass spectrum acquired in negative ion mode for an aqueous ammonium acetate solution (200 mM, 25 °C and pH 6.8) of $Stx1B_5$ (3 μM) with 320 μM GM3. (b) CID mass spectrum measured for ions produced by ESI for the solutions described in (a). Ions within a window of m/z values (~50 m/z units wide) centred at m/z 3,993 (which corresponds to the -10 charge state of $Stx1B_5$ bound to GM3) were isolated and subjected to CID in the Trap using a collision energy of 100 V. Peaks labeled with * correspond to CID fragment ions produced from impurities in $Stx1B_5$ sample.

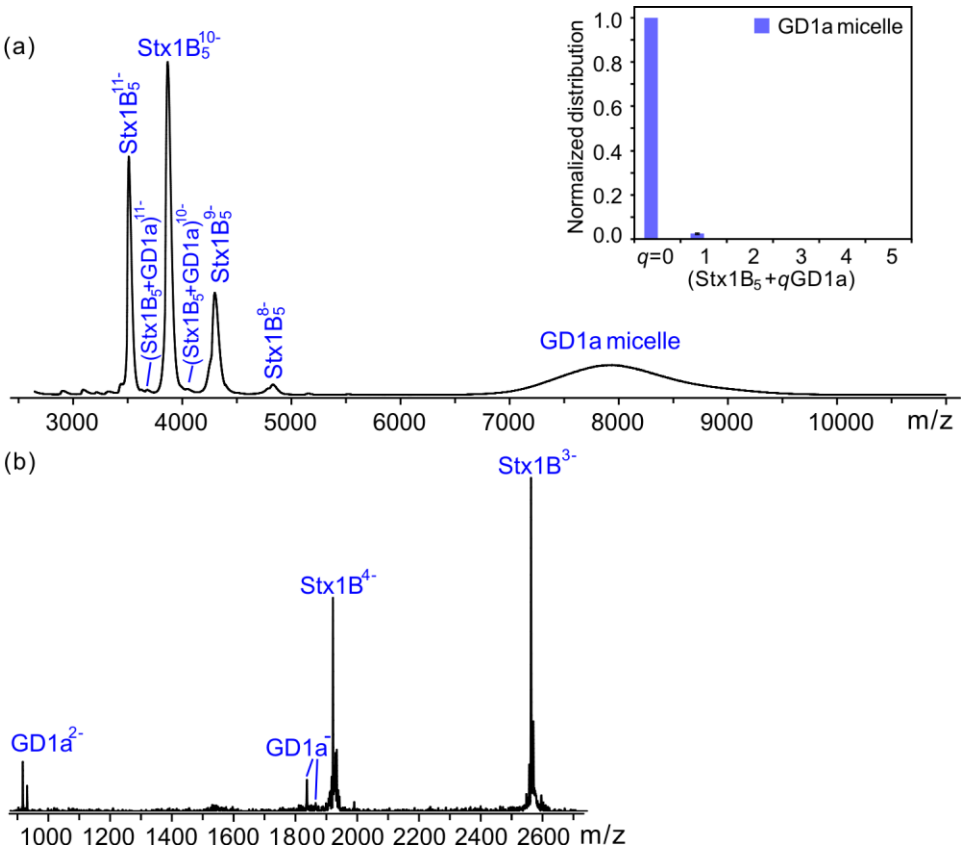

Figure S15. (a) ESI mass spectrum acquired in negative ion mode for an aqueous ammonium acetate solution (200 mM, 25 °C and pH 6.8) of $Stx1B_5$ (3 μM) with 320 μM GD1a. Inset shows the normalized distributions of free and GD1a-bound $Stx1B_5$; the reported errors correspond to one standard deviation. (b) CID mass spectrum measured for ions produced by ESI for the solutions described in (a). Ions within a window of m/z values (~50 m/z units wide) centred at m/z 4,055 (which corresponds to the -10 charge state of $Stx1B_5$ bound to GD1a) were isolated and subjected to CID in the Trap using a collision energy of 100 V.

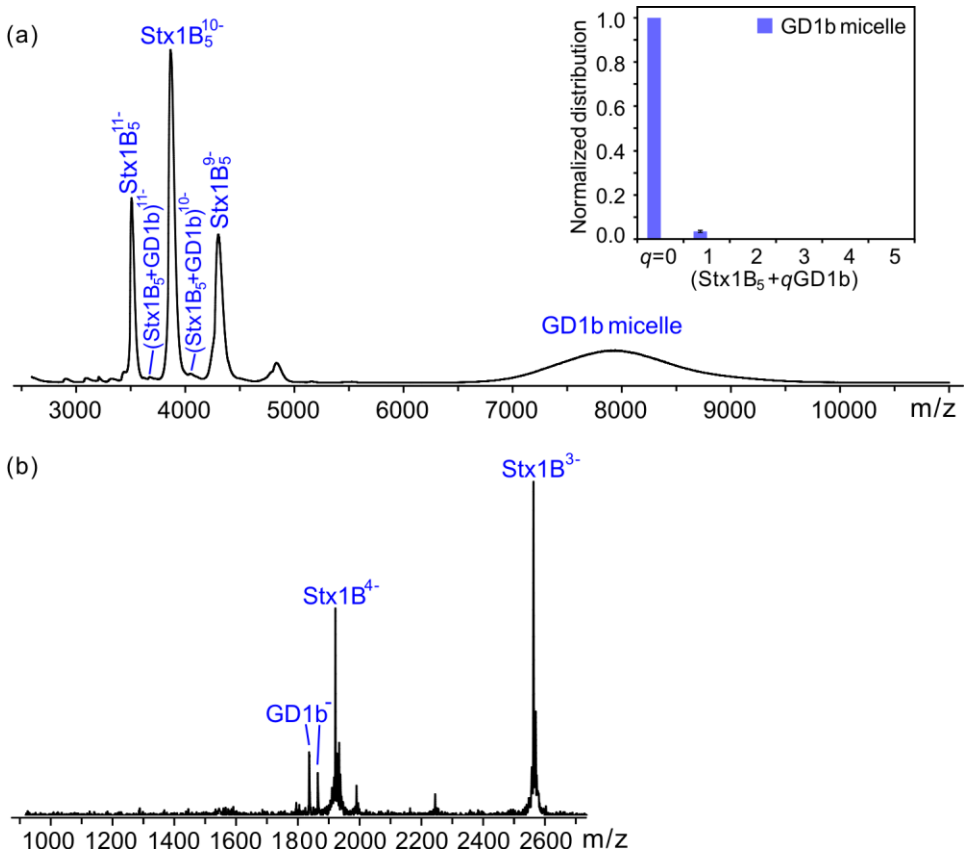

Figure S16. (a) ESI mass spectrum acquired in negative ion mode for an aqueous ammonium acetate solution (200 mM, 25 °C and pH 6.8) of $Stx1B_5$ (3 µM) with 320 µM GD1b. Inset shows the normalized distributions of free and GD1b-bound Stx1B; the reported errors correspond to one standard deviation. (b) CID mass spectrum measured for ions produced by ESI for the solutions described in (a). Ions within a window of m/z values (~50 m/z units wide) centred at m/z 4,055 (which corresponds to the -10 charge state of $Stx1B_5$ bound to GD1b) were isolated and subjected to CID in the Trap using a collision energy of 100 V.

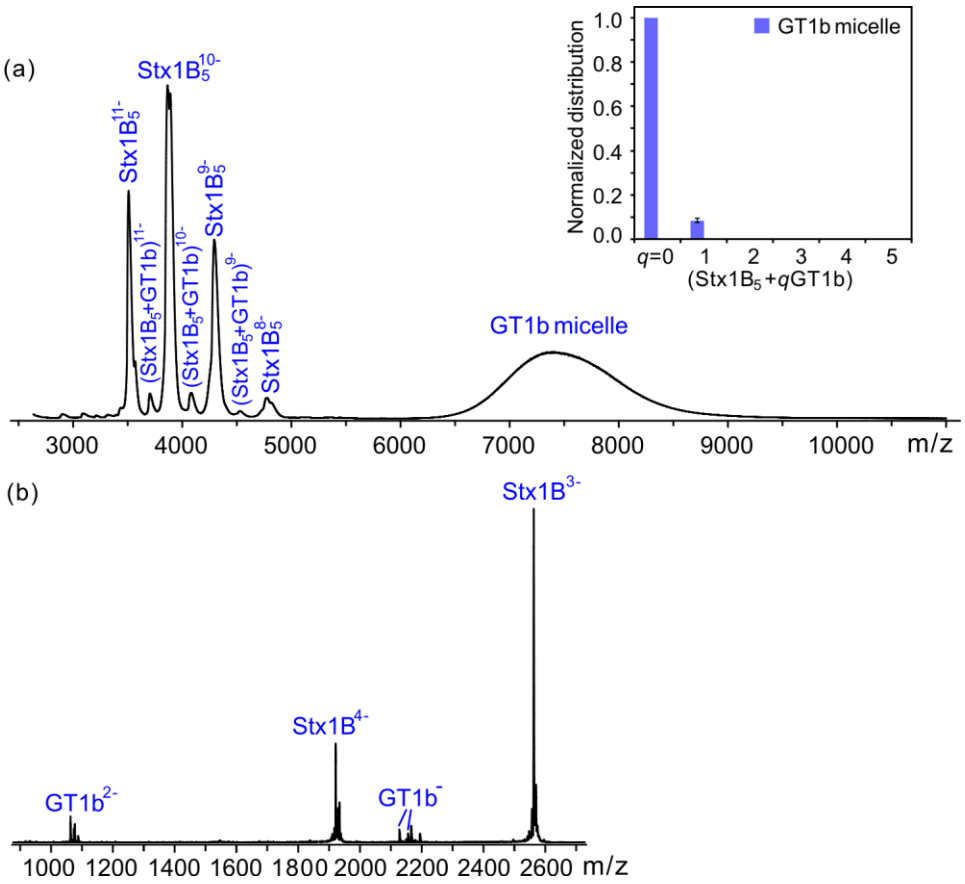

Figure S17. (a) ESI mass spectrum acquired in negative ion mode for an aqueous ammonium acetate solution (200 mM, 25 °C and pH 6.8) of $Stx1B_5$ (3 µM) with 320 µM GT1b. Inset shows the normalized distributions of free and GT1b-bound $Stx1B_5$; the reported errors correspond to one standard deviation. (b) CID mass spectrum measured for ions produced by ESI for the solutions described in (a). Ions within a window of m/z values (~50 m/z units wide) centred at m/z 4,085 (which corresponds to the -10 charge state of $Stx1B_5$ bound to GT1b) were isolated and subjected to CID in the Trap using a collision energy of 100 V.

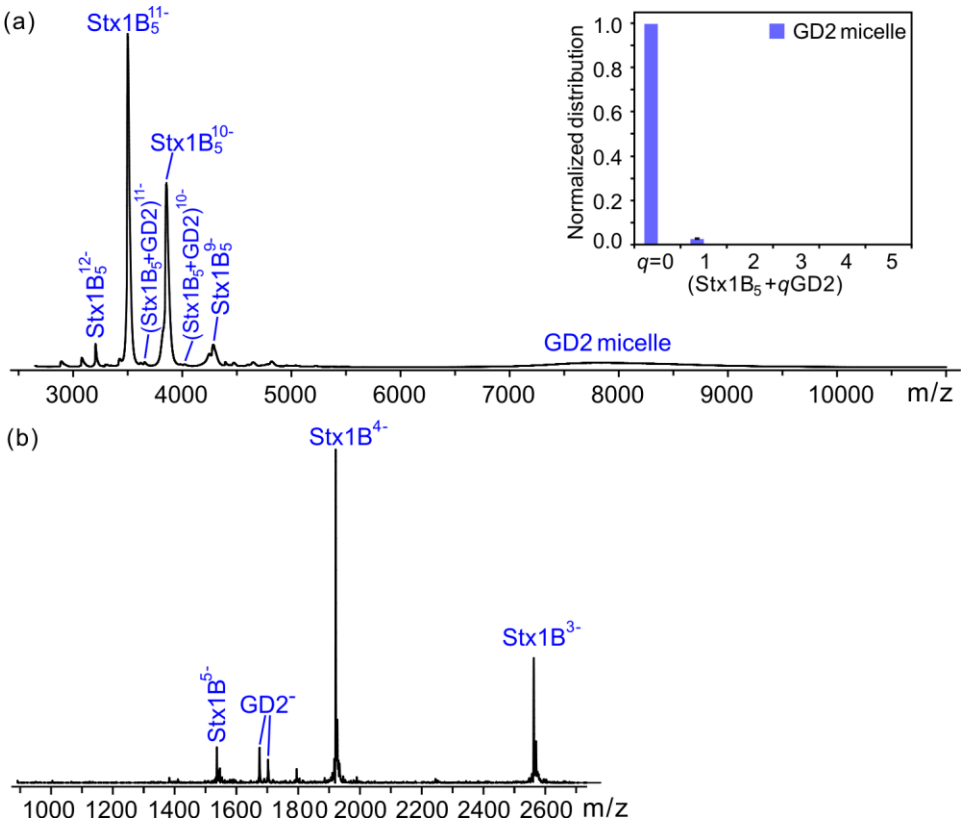

Figure S18. (a) ESI mass spectrum acquired in negative ion mode for an aqueous ammonium acetate solution (200 mM, 25 °C and pH 6.8) of $Stx1B_5$ (3 µM) with 320 µM GD2. Inset shows the normalized distributions of free and GD2-bound $Stx1B_5$; the reported errors correspond to one standard deviation. (b) CID mass spectrum measured for ions produced by ESI for the solutions described in (a). Ions within a window of m/z values (~50 m/z units wide) centred at m/z 4,044 (which corresponds to the -10 charge state of $Stx1B_5$ bound to GD2) were isolated and subjected to CID in the Trap using a collision energy of 100 V.

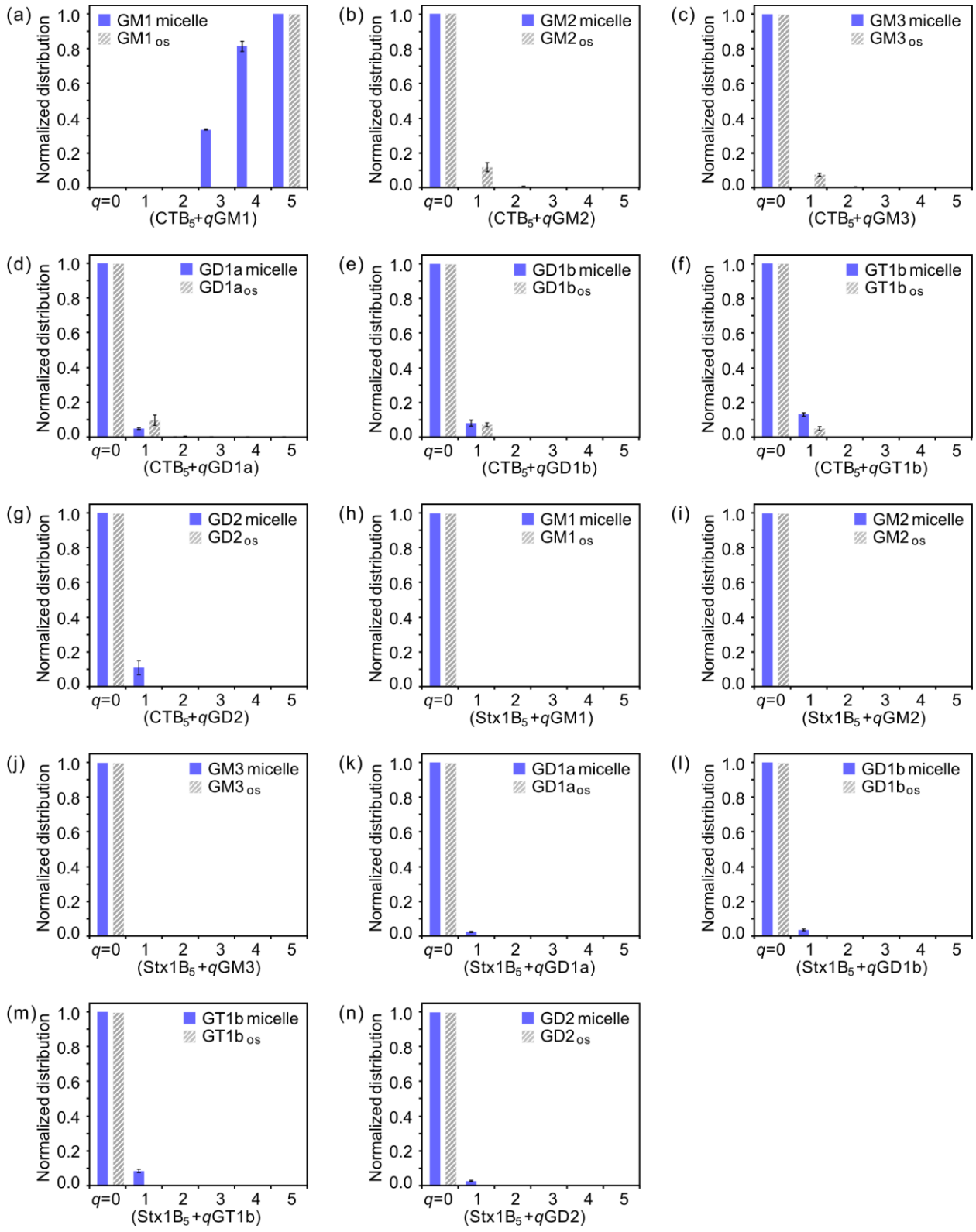
(a)
GM1 micelle
GM1 os
Normalized distribution
(CTB5+qGM1)
(b)
GM2 micelle
GM2 os
(CTB5+qGM2)
(c)
GM3 micelle
GM3 os
(CTB5+qGM3)
(d)
GD1a micelle
GD1aos
(CTB5+qGD1a)
(e)
GD1b micelle
GD1bos
(CTB5+qGD1b)
(f)
GT1b micelle
GT1b os
(CTB5+qGT1b)
(g)
GD2 micelle
GD2 os
(CTB5+qGD2)
(h)
GM1 micelle
GM1 os
(Stx1B5+qGM1)
(i)
GM2 micelle
GM2 os
(Stx1B5+qGM2)
(j)
GM3 micelle
GM3 os
(Stx1B5+qGM3)
(k)
GD1a micelle
GD1aos
(Stx1B5+qGD1a)
(l)
GD1b micelle
GD1bos
(Stx1B5+qGD1b)
(m)
GT1b micelle
GT1b os
(Stx1B5+qGT1b)
(n)
GD2 micelle
GD2 os
(Stx1B5+qGD2)
q=0 1 2 3 4 5
0.0 0.2 0.4 0.6 0.8 1.0

Figure S19. (a)–(g) Normalized distributions of free and ganglioside-bound CTB_5 measured by ESI-MS performed on 200 mM aqueous ammonium acetate solutions (25 °C and pH 6.8) containing 3 μM CTB_5 and 200 μM each of the ganglioside. The reported errors correspond to one standard deviation. Also shown are the corresponding distributions of bound ganglioside oligosaccharides expected based on the association constants reported in (a) reference S4 or (b)–(g) reference S3; the errors were calculated from propagation of uncertainties in the reported association constants. (h)–(n) Normalized distributions of free and ganglioside-bound $Stx1B_5$ measured by ESI-MS performed on 200 mM aqueous ammonium acetate solutions (25 °C and pH 6.8) containing 3 μM $Stx1B_5$ and 320 μM each of the ganglioside. Also shown are the distributions of corresponding bound ganglioside oligosaccharides expected based on the binding results reported in the present work (which revealed no binding between $Stx1B_5$ and the ganglioside oligosaccharides).

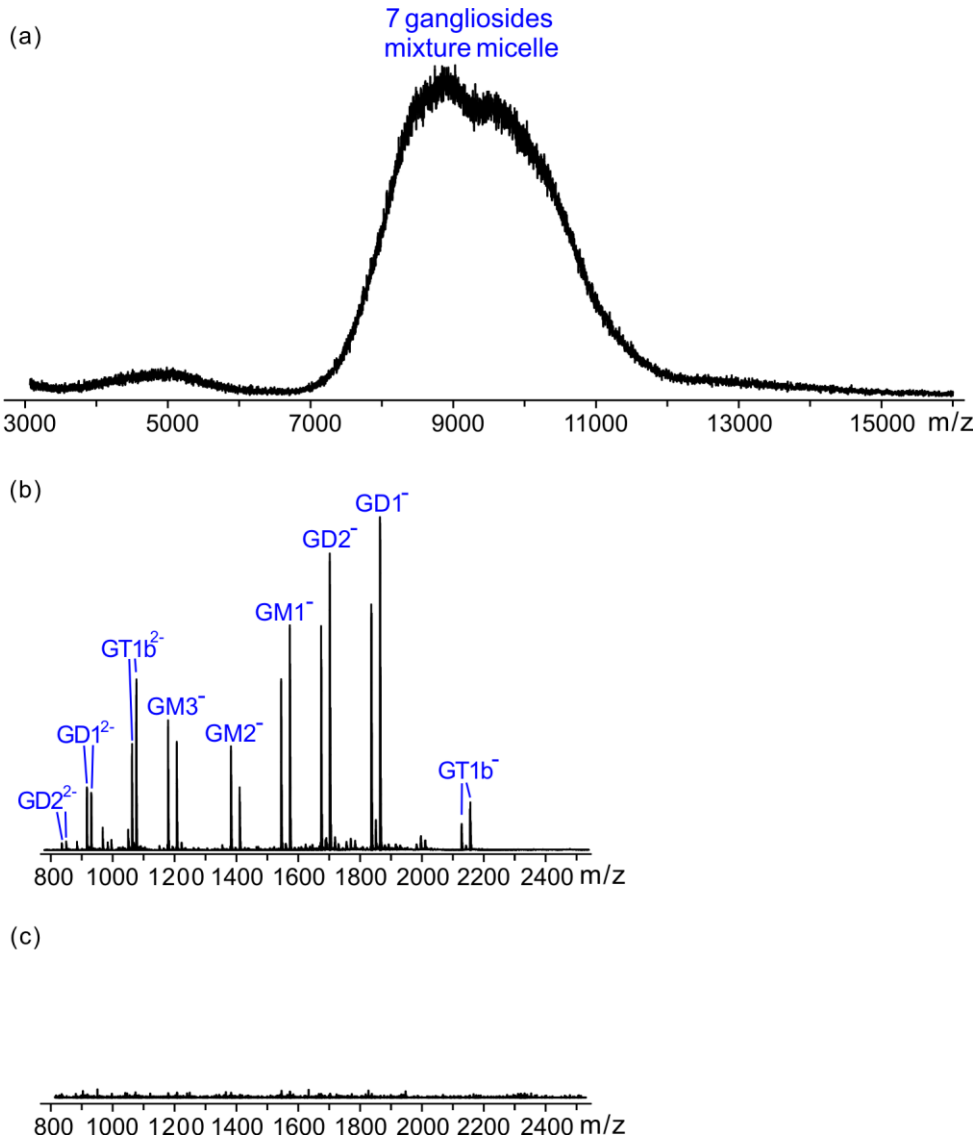

Figure S20. (a) ESI mass spectrum acquired in negative ion mode for an aqueous ammonium acetate solution (200 mM, 25 °C and pH 6.8) of GM1, GM2, GM3, GD1a, GD1b, GT1b and GD2, each at 170 μM. (b) and (c) CID mass spectra measured for ions produced by ESI for the solutions described in (a). (b) Ions within a window of m/z values (~200 m/z units wide) centred at m/z 9,000 were isolated and subjected to CID in the Trap using a collision energy of 100 V. (c) Ions within a window of m/z values (~100 m/z units wide) centred at m/z 4,400 were isolated and subjected to CID in the Trap using a collision energy of 100 V.

References

S1. Sun, J., Kitova, E.N., Wang, W., Klassen, J.S.: Method for distinguishing specific from nonspecific protein-ligand complexes in nanoelectrospray ionization mass spectrometry. Anal. Chem. **78**, 3010-3018 (2006)

S2. Kitova, E., El-Hawiet, A., Schnier, P., Klassen, J.: Reliable determinations of protein–ligand interactions by direct ESI-MS measurements. Are we there yet? J. Am. Soc. Mass. Spectrom. **23**, 431-441 (2012)

S3. Li, J., Fan, X., Kitova, E.N., Zou, C., Cairo, C.W., Eugenio, L., Ng, K.K.S., Xiong, Z.J., Privé, G.G., Klassen, J.S.: Screening glycolipids against proteins in vitro using picodiscs and catch-and-release electrospray ionization mass spectrometry. Anal. Chem. **88**, 4742-4750 (2016)

S4. Lin, H., Kitova, E.N., Klassen, J.S.: Measuring positive cooperativity using the direct ESI-MS assay. Cholera toxin B subunit homopentamer binding to GM1 pentasaccharide. J. Am. Soc. Mass. Spectrom. **25**, 104-110 (2013)